8-23-91
E 5660

NASA
Technical
Paper
3142

August 1991

Evaluation of a Technique To Generate Artificially Thickened Boundary Layers in Supersonic and Hypersonic Flows

A. R. Porro,
W. R. Hingst,
D. O. Davis,
and A. B. Blair, Jr.

NASA

NASA Technical Paper 3142

1991

Evaluation of a Technique To Generate Artificially Thickened Boundary Layers in Supersonic and Hypersonic Flows

A. R. Porro and W. R. Hingst
Lewis Research Center
Cleveland, Ohio

D. O. Davis
University of Washington
Seattle, Washington

A. B. Blair, Jr.
Langley Research Center
Hampton, Virginia

NASA
National Aeronautics and Space Administration
Office of Management
Scientific and Technical Information Program

Summary

The feasibility of using a contoured honeycomb model to generate a thick boundary layer in high-speed, compressible flow has been investigated. The contour of the honeycomb was tailored to selectively remove momentum in a minimum of streamwise distance to create an artificially thickened turbulent boundary layer. Three wind tunnel experiments were conducted to verify the concept. The first experiment documented the momentum profile and turbulence levels of an artificially thickened boundary layer when tested at nominal Mach numbers of 3.0, 3.5, and 4.0. The second experiment used the concept to generate a thick boundary layer in a channel flow configuration at the same Mach numbers. Oblique-shock—boundary-layer interactions were investigated, along with pure channel flow. Comparisons were made between the simulated boundary layer and a thick, naturally occurring turbulent boundary layer. The third experiment extended the application of the technique to Mach 6. Both schlieren and surface oil flow visualization were used to qualitatively assess the performance of the honeycomb boundary layer simulator. Surface static pressures, together with pitot pressure, static pressure, and hot-wire anemometry flow-field measurements were used to quantify the performance of the boundary layer simulation technique. Results indicate that this technique is a viable concept, especially for high-speed inlet testing applications. In addition, the compactness of the honeycomb boundary layer simulator allows relatively easy integration into existing wind tunnel model hardware. However, Mach number and total pressure losses associated with the boundary layer simulation process must be considered when using the technique.

Introduction

Hypersonic vehicles are often designed with the propulsion system inlets integrated into the vehicle. Because such vehicles have long forebodies, very thick boundary layers are ingested into the inlets. Accurate testing of these propulsion systems in high-speed wind tunnels requires that the entire forebody-inlet system be modeled. In situations where modeling of the complete forebody is not feasible, an alternate method must be developed to simulate the thick forebody boundary layers entering the propulsion system inlet. Ideally, this should be done without compromising the scale of the propulsion system. Therefore, it is desirable to simulate the forebody boundary layer by a method that would shorten the overall length of the test model.

The objective of this investigation is to develop and experimentally test a technique for generating thick boundary layers in supersonic flow over a minimum streamwise distance. Ideally, these boundary layers should have the momentum and turbulence distribution that would be expected from a naturally occurring turbulent boundary layer.

To develop the simulated boundary layers in this experimental program, a metal honeycomb material is placed in a supersonic flow. The cell length of the honeycomb material is varied in the transverse direction to selectively remove momentum as a function of distance from the wall. The flow through the individual honeycomb cells is assumed to follow the Fanno line process. The goal is to tailor the momentum removal to match that of a naturally occurring boundary layer. Previous attempts to generate artificially thickened boundary layers have used cylindrical or conical protuberances to thicken a naturally occurring boundary layer (refs. 1 and 2). The use of the honeycomb has the potential to provide a technique that has better control of the momentum distribution while maintaining ease of installation.

This investigation involved three separate experiments: an isolated boundary layer simulator test and a channel flow test conducted in the 1- by 1-Foot Supersonic Wind Tunnel (SWT) at NASA Lewis Research Center, and a channel flow test in the 20 Inch—Mach 6 Hypersonic Wind Tunnel (HWT) at NASA Langley Research Center. The isolated boundary layer simulator test was regarded as a proof-of-concept experiment, to answer questions about the structural integrity and starting characteristics of the model, as well as to measure the downstream Mach number and turbulence profiles that were generated. The second experiment applied the concept to an internal flow application. This test investigated the downstream development of a simulated boundary layer in a channel and evaluated the behavior of this boundary layer interacting with an oblique shock. This tested the ability of the technique to simulate interactions that are common in supersonic inlet flows. The third experiment used a channel flow model similar to that used in the previous investigation, but was conducted at a higher Mach number. Because the Langley tunnel had larger test section dimensions, a larger model could be tested in this experiment.

Symbols

D characteristic diameter of honeycomb cell (0.635 cm)

H model height characteristic dimension

M Mach number

P total or pitot pressure

p static pressure

Re Reynolds number, $\frac{\rho u x}{\mu}$

S model span characteristic dimension

U_e boundary layer edge velocity

u axial component of velocity

u_τ wall-friction velocity, $\sqrt{\tau_w/\rho_w}$

u' rms fluctuating component of the axial velocity

x axial (streamwise) coordinate relative to trailing edge of the boundary layer simulator

y height (transverse) coordinate relative to model floor

z width (spanwise) coordinate relative to model right sidewall

α cowl wedge angle

δ boundary layer thickness

ρ fluid density

τ shear stress

Subscripts:

eff effective height

h/c boundary layer simulator

nb naturally occurring boundary layer

o total or plenum conditions

s,u tunnel reference static pressure

t local pitot pressure

w wall property value

Experimental Approach

Facilities

The first two experiments were conducted in the NASA Lewis Research Center 1- by 1-Foot Supersonic Wind Tunnel (fig. 1(a)). This continuous-running wind tunnel has a Mach number range of 1.3 to 4.0. Tunnel total pressures can be varied from 1 to 3 atm to give a unit Reynolds number range from 12.0×10^6 to 24.0×10^6/m. The tunnel test section dimensions are 30.5 by 31.0 cm. A detailed description of the tunnel is given in reference 3.

The third experiment was conducted in the NASA Langley Research Center 20 Inch—Mach 6 Hypersonic Wind Tunnel (fig. 1(b)). The facility is a blowdown tunnel with typical run times of 7 min for the conditions of the present study. This tunnel is capable of producing flows with Reynolds numbers of up to 29.5×10^6/m. In this investigation, the tunnel total pressure variation was from 15 to 29 atm with total temperature variations from 470 to 490 K. These conditions produce unit Reynolds numbers from 13.1×10^6 to 23.0×10^6/m. The tunnel test section dimensions are 52.1 by 50.8 cm. A detailed discussion of the facility can be found in reference 4.

The first two experiments were conducted within a Mach number range of 3.0 to 4.0 with unit Reynolds numbers approaching 16.0×10^6/m. The third experiment was conducted at a Mach number of 6.0 with unit Reynolds numbers approaching 23.0×10^6/m. In this report, the Mach numbers referred to are nominal values. The actual Mach numbers and test conditions are listed in table I.

Experimental Configurations

Two basic models are used in this investigation: an isolated boundary layer simulator model, and two variations of a channel flow model. The model coordinate system used in this study for all experimental configurations is shown in figure 2. The origin of the coordinate system is at the trailing edge of the boundary layer simulator along the left sidewall.

A typical boundary layer simulator is shown in figure 3(a). The simulator is permanently mounted on a base plate which is fastened to the flat plate or channel flow model. This mounting facilitates the changing of boundary layer simulator configurations. All boundary layer simulators in this investigation are constructed of stainless steel honeycomb with a characteristic hexagonal cell diameter of 0.635 cm. For the experiments conducted in the NASA Lewis 1- by 1-Foot SWT, the honeycomb material is bonded to the base plate with an epoxy material. Because of the higher tunnel total temperatures encountered when testing at Mach 6, the honeycomb is spot-welded to the base plate.

The boundary layer simulator shown in the figure is an early version. In addition to the sidewall supports, it has a cross-member attached to the top of the honeycomb material to insure structural integrity. Initial measurements indicated that this member generated a substantial shock wave, which adversely affected the simulated boundary layer. Therefore, all subsequent boundary layer simulators were constructed and tested without the top member. No structural failures occurred with the top member missing.

A schematic of the isolated boundary layer simulator model is shown in fig. 3(b). This model has a boundary layer simulator mounted near the leading edge of a flat plate. The plate is installed in the NASA Lewis 1- by 1-Foot SWT and spans the entire test section. The honeycomb boundary layer simulator does not span the complete tunnel so that the naturally

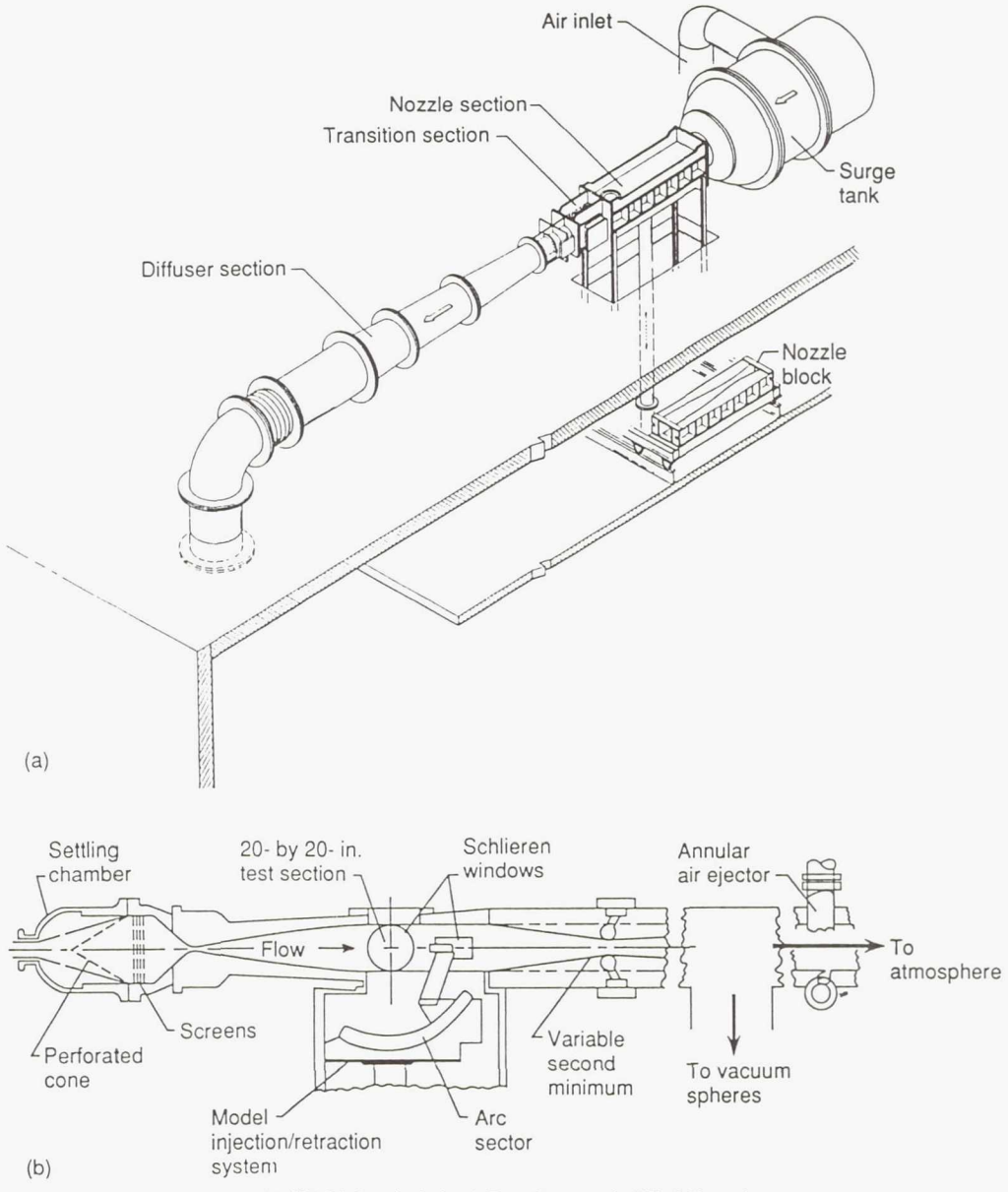

(a) NASA Lewis 1- by 1-Foot Supersonic Wind Tunnel.
(b) NASA Langley 20 Inch—Mach 6 Hypersonic Wind Tunnel.

Figure 1.—Experimental facilities.

TABLE I.—RUN CONDITIONS

Nominal Mach number	Actual Mach number	Tunnel total pressure, P_0, kPa	Tunnel reference static pressure, $p_{s,0}$, kPa	Per meter Reynolds number
3.0	2.96	207	5.98	15.7×10^6
3.5	3.47	241	3.30	14.2
4.0	3.96	276	1.92	12.9
6.0	5.97	1550	1.01	13.1
6.0	5.99	2070	1.32	17.2
6.0	6.00	2930	1.86	23.0

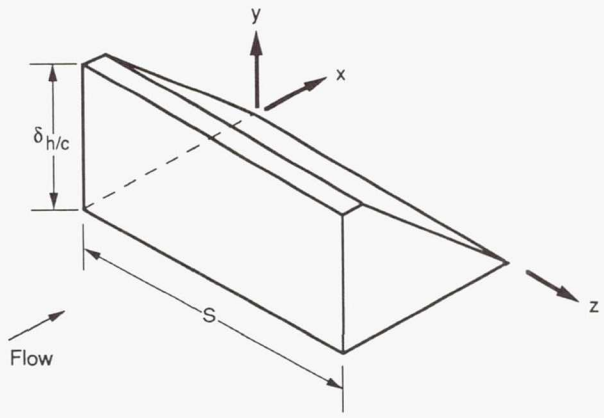

Figure 2.—Model coordinate system.

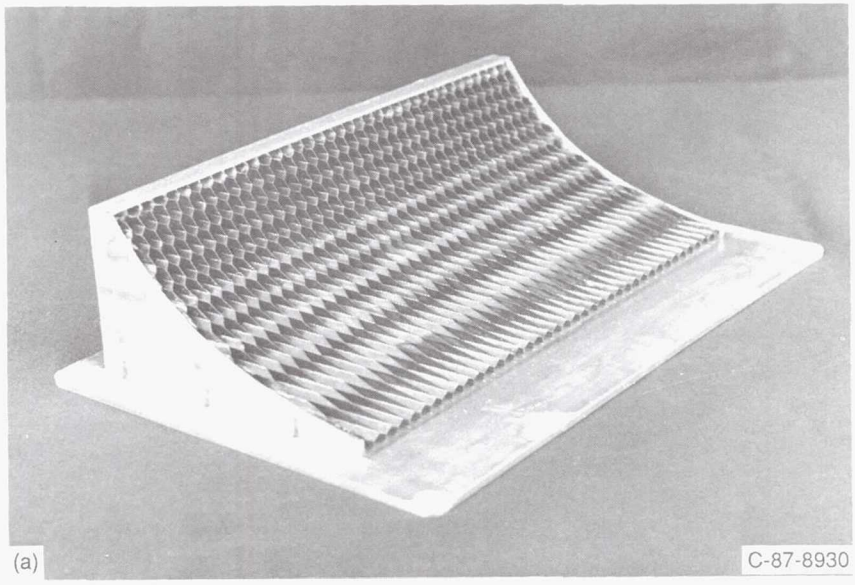

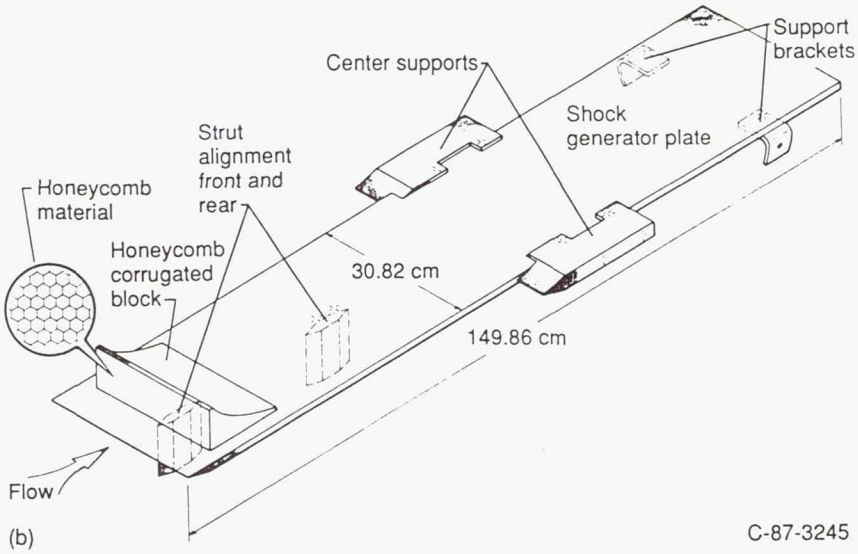

(a) Honeycomb.
(b) Schematic.

Figure 3.—Isolated boundary layer simulator model.

occurring sidewall boundary layers would not be ingested. The model could be moved in the streamwise direction to allow optical access at more than one position downstream of the boundary layer simulator. Access holes located in the test section wall opposite the flat plate are used for probing the flow downstream of the boundary layer simulator.

Since the isolated boundary layer simulator model experiment was regarded as a proof-of-concept test, several configurations were investigated. The first two configurations used a boundary layer simulator with a contoured cross section. The shape of the contour was determined by using a Fanno line analysis to selectively remove momentum to create an artificially thickened boundary layer that matched a turbulent boundary layer power profile. For this contour, two boundary layer simulator heights were considered: 4.06 and 6.35 cm. The reduced-height boundary layer simulators were 25.2 cm wide, and the 6.35-cm-high simulator was 20.32 cm wide. Based on the preliminary results from these configurations, a third boundary layer simulator was designed which had a linear cross section; that is, a linear taper was used in the transverse direction from the longest cell (at the model floor) to the shortest cell. Its height was 4.06 cm. The preliminary results indicated similar performance between the contoured and linear taper cross-section boundary layer simulators. Because of the similar performance and ease of manufacture, the linear taper contour was chosen for all subsequent experiments.

The channel flow model used in the NASA Lewis 1- by 1-Foot SWT experiments is shown in figure 4. The boundary

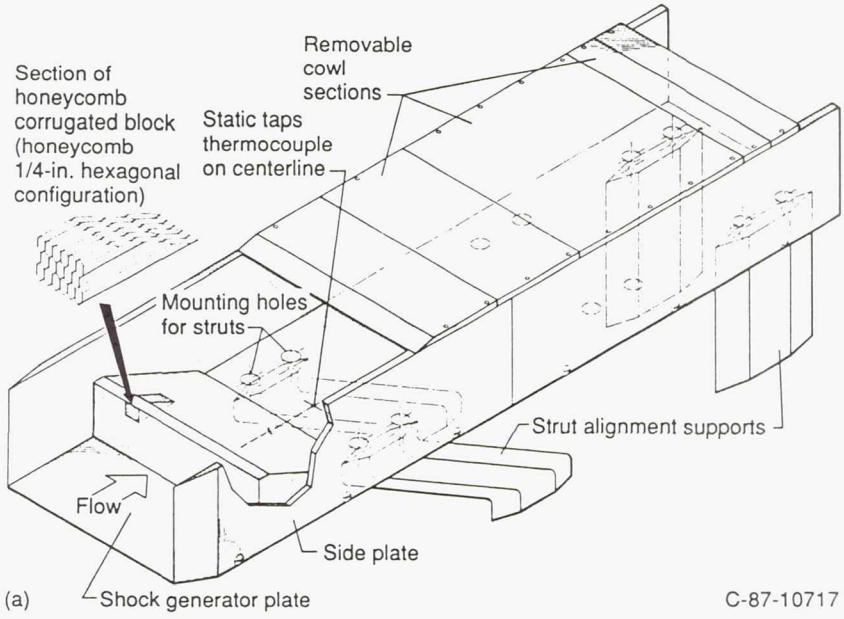

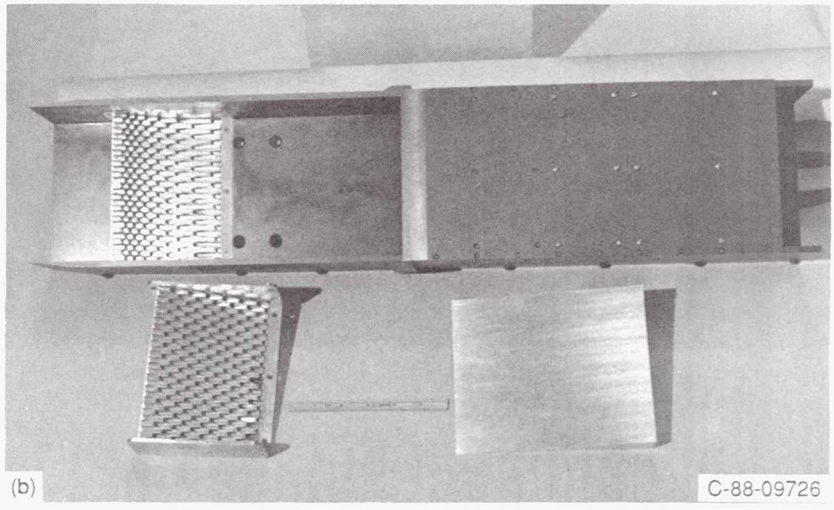

(a) Schematic.
(b) Model hardware.

Figure 4.—NASA Lewis channel flow model.

layer simulator is mounted in a channel 15.24 cm wide and 7.62 cm high. Its height corresponds to 53.3 percent of the channel height. As with the first experiment, the boundary layer simulator is mounted on a base plate. This allows a blank insert to be used in place of the honeycomb boundary layer simulator when ingesting the naturally occurring tunnel sidewall boundary layers into the channel. The overall length of the model is 76.20 cm, and the distance between the trailing edge of the boundary layer simulator and the end of the channel is equivalent to 88 honeycomb cell diameters. A cowl is installed on the channel model to isolate the internal flow from external flow disturbances. Its leading edge is located 30 cell diameters downstream of the boundary layer simulator trailing edge. The cowl is at a 0° angle of attack and does not generate any substantial shock. This model is similar to an inlet application, although there is no internal compression in this configuration. A modification of this model is obtained by installing wedges on the inside of the cowl surface to produce oblique shocks that would interact with the boundary layer in the channel.

The channel flow model can be mounted in two positions. The illustration in fig. 4(a) depicts the channel on strut supports for mounting at the tunnel midspan location. An alternate configuration allows the model without the boundary layer simulator installed to be mounted with the leading edge flush with the tunnel sidewall. The naturally occurring tunnel sidewall boundary layer is then ingested into the channel, allowing a comparison to be made between naturally occurring and simulated boundary layer behavior.

The final model used in the investigation is the channel model which was tested in the NASA Langley Research Center 20 Inch—Mach 6 HWT. This model, shown in figure 5, is similar to the one tested in the Lewis 1- by 1-Foot SWT, but it is scaled up in order to take advantage of the larger test section. The channel dimensions are 29.21 cm wide and 8.89 cm high. Two interchangeable boundary layer simulator inserts corresponding to 43 and 57 percent of the channel height are used to generate the simulated boundary layer. The model is built in two parts so that the floor of the channel upstream of the cowl is replaceable. This feature allows cross-plane flow-field surveys at two axial locations in the model. The long configuration, shown in figure 5(a), is 101.6 cm in length, whereas the short configuration, shown in figure 5(b), is 76.2 cm. When testing the long configuration, a cowl is installed such that the leading edge is located 96 cell diameters downstream of the boundary layer simulator. The cowl, which is 20.32 cm long, is mounted at a 0° angle of attack so that no substantial shock is generated in the channel. Use of the two configurations allows flow-field surveys at locations equivalent to 10 honeycomb cell diameters upstream and 30 cell diameters downstream of the cowl leading edge.

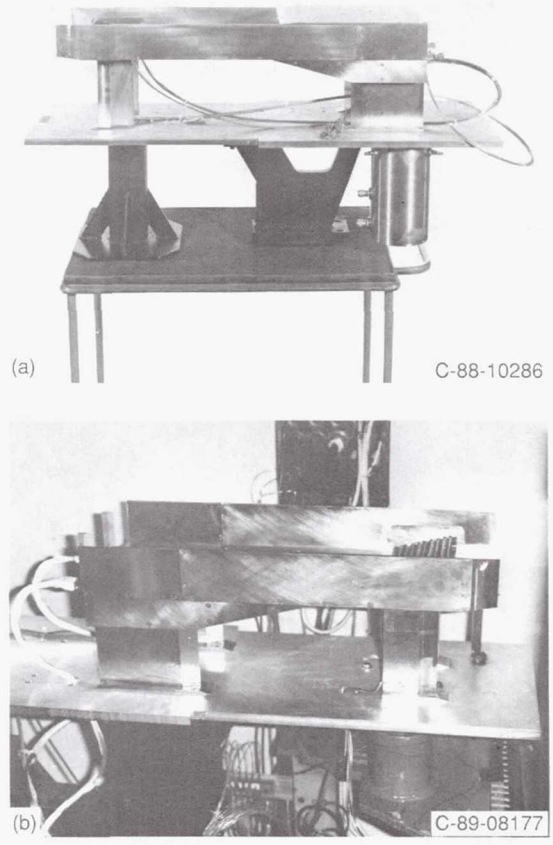

(a) Cowl exit survey plane configuration.
(b) Cowl upstream survey plane configuration.

Figure 5.—NASA Lewis/Langley channel flow model.

Instrumentation and Experimental Technique

This investigation uses both qualitative measurement techniques and quantitative instrumentation. The flow visualization techniques include schlieren and surface oil flow. The schlieren technique, which visually shows the density gradients, provides an integrated two-dimensional picture representative of the free-stream flow. In contrast, the surface oil flow visualization indicates flow direction at the model surface. The combination of these techniques is useful in determining shock structure and flow separation.

A schlieren system was used in both the Lewis 1- by 1-Foot SWT and the Langley 20 Inch—Mach 6 HWT. The schlieren photographs represent a steady-state visualization of the flow since the exposure time is long compared to the frequencies of any flow instability. The surface oil flow visualization used a petroleum-based oil with an SAE viscosity rating of 140 which was mixed with a fluorescent dye. After a test run, the flow surface was illuminated with an ultraviolet light source and then photographed. This highlighted the oil flow while suppressing the wall reflections. Because of the high viscosity of the oil, the run conditions were held for several minutes to allow the oil to stabilize. The high viscosity also minimized oil flow during tunnel shutdown. The technique was used in both wind tunnels. A detailed description of this technique is given in reference 5.

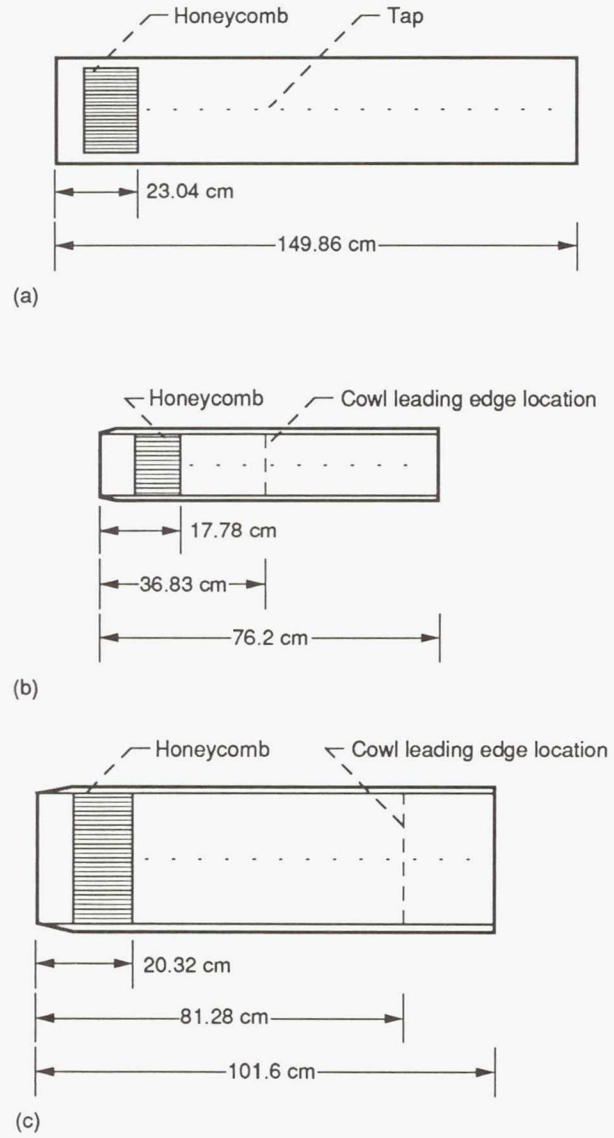

(a) Isolated boundary layer simulator model (24 taps equally spaced at 5.08 cm; tap 1 is 5.08 downstream of honeycomb trailing edge).
(b) NASA Lewis channel flow model (22 taps equally spaced at 2.54 cm; tap 1 is 2.54 cm downstream of honeycomb trailing edge).
(c) NASA Lewis/Langley channel flow model (tap 1 is 3.87 cm downstream of honeycomb trailing edge; taps 1 to 23 and 25 to 31 equally spaced at 2.54 cm; tap 24 is 3.3 cm downstream of tap 23; tap 25 is 1.91 cm downstream of tap 24).

Figure 6.—Schematic of model hardware static tap locations.

Quantitative measurements consisted of surface static pressures and flow-field surveys. The surface static taps for all models include streamwise taps along the model floor centerline. Figure 6 shows the location of the wall static pressure taps for each model. In both tunnels, all pressure measurements were made with an electronically scanned pressure measurement system. Wall static pressure measurements were made with the probe or rake positioned so they would not affect the model surface static pressures.

Flow-field surveys for the isolated boundary layer simulator model included pitot pressure and hot-wire anemometer measurements. The probe actuation system allowed the pressure and hot-wire probes to survey in the transverse direction at various streamwise locations at the mounting plate centerline. This produced an x-y survey plane downstream of the boundary layer simulator. For measurements that used an actuated probe, an electronic touch control was used to indicate wall location. All boundary layer distances from the wall were measured relative to this touch value. This provided an accurate distance for all boundary layer measurements and removed any error caused by probe deflection due to aerodynamic loading.

Additional hot-wire measurements were made on the 1- by 1-Foot SWT sidewall without the model installed. These measurements were used as a baseline for comparison with the measurements downstream of the boundary layer simulator; that is, the tunnel sidewall boundary layer can be considered a naturally occurring equilibrium turbulent boundary layer. The sidewall hot-wire measurements were made at one streamwise location in the tunnel.

The hot-wire measurements in the 1- by 1-Foot SWT were restricted to streamwise fluctuating components. The hot-wire was calibrated in the empty wind tunnel. The calibration and data reduction technique followed the approach of reference 6. The mass flux sensitivity was determined directly from measurement of the wire response over a range of Mach numbers, Reynolds numbers, and overheat ratios. The total temperature sensitivity was determined indirectly from an empirical relation. The measurement of the boundary layer fluctuating quantities involved repeated surveys at five overheat ratios. Although this approach is somewhat laborious, the data reduction requires fewer assumptions about the hot-wire response.

The flow-field surveys for the two channel flow models consisted of sequential pitot and static rake surveys at various cross planes in the channel. These rakes were aligned in the transverse direction and actuated in the spanwise direction which resulted in y-z survey planes. The actuation systems differed between the two models. The 1- by 1-Foot SWT system was sting-mounted from the tunnel, whereas the system used in the 20 Inch—Mach 6 HWT test was contained within the model. The Mach 6 model used two rakes in order to obtain a full-span traverse.

Flow-field surveys were made with interchangeable pitot and static pressure rakes. In the Lewis channel flow model, a sting-mounted actuator was used to move a single rake in the spanwise direction at a constant channel axial location which constituted a survey plane. The actuation system could reposition the rake to conduct surveys at numerous axial planes. During a typical run, the 1- by 1-Foot SWT was brought on condition with the rake positioned just downstream of the channel. The rake was moved axially to the first survey plane in the channel, and a remotely controlled actuation system stepped the rake across the channel span in predetermined increments. When the rake traversed to a new spanwise location, a data point was recorded after a short waiting period

in order to let the rake pressure fluctuations due to the rake movement settle out. After the survey was completed at a channel cross plane, the actuator moved the rake upstream to a new axial location, and the process was repeated.

In the case of the NASA Lewis/Langley channel flow model, cross-plane flow-field surveys were conducted in a similar manner. However, since the Langley 20 Inch—Mach 6 HWT is a blowdown facility, survey time constraints required the use of two rakes to conduct a full-span traverse of the channel. In addition, the rake actuation system was integrated in the test model; therefore, only one cross-plane rake survey was made during a tunnel run. As mentioned earlier, the model hardware was changed in order to conduct flow-field surveys at two channel crossplanes.

Experimental Results

Qualitative Results

Qualitative results include those of the schlieren and surface oil flow visualization techniques. Figure 7 shows the schlieren results at Mach 4.0 for the isolated boundary layer simulator experiment. The linear cross section of the boundary layer simulator can be seen. In addition, the characteristics of the exiting flow are seen downstream of the boundary layer simulator. Two families of waves are seen in the schlieren. Mach lines are indicated and are at an angle relative to the tunnel flow. These are associated with the adjustment of the flow exiting from the model. As the thick boundary layer is generated, the displacement thickness increases. This rapid change in the displacement thickness must affect the free-stream flow, as shown by the compression fan exiting the model. The second family of waves is parallel to the main flow and is associated with the mixing of various layers emerging from the individual cells of the model at different velocities. These layers mix as they proceed downstream of the boundary layer simulator and form the characteristic velocity distribution of boundary layer flow.

As discussed previously, the model could be moved streamwise in the tunnel by repositioning the mounting plate. Figure 8 shows a composite of two photographs with the model in two positions. The coalescence of the compression fan into a shock wave can be seen in this composite photo.

The surface oil flow results are presented only for representative test conditions. Figure 9 shows surface oil flow patterns on the floor of the NASA Lewis/Langley Mach 6 channel flow model. The test condition is at a tunnel nominal Mach number of 6 and a unit Reynolds number of 13.1×10^6/m. The view is looking down on the channel from above, and the flow is from left to right. A separation line can be seen just upstream of the boundary layer simulator. Flow separation may occur because the incoming thin laminar boundary layer "feels" the effect of minute discontinuities at the honeycomb/model floor juncture. Inspection of corresponding schlieren photographs shows no strong shock system present in the vicinity of this separation. The separation appears to be localized and close to the model surface. The surface oil patterns downstream of the honeycomb indicate that the flow is well-behaved, since no patterns indicating a large-scale flow separation are present.

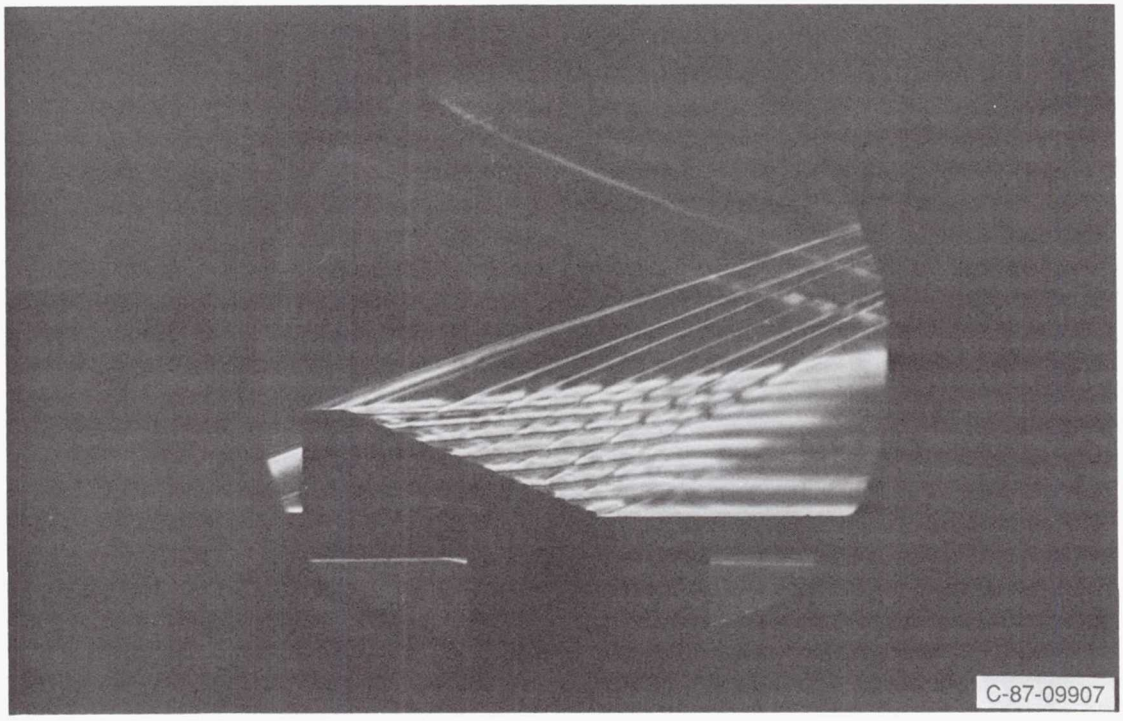

Figure 7.—Schlieren photograph of isolated boundary layer simulator at Mach 4.0.

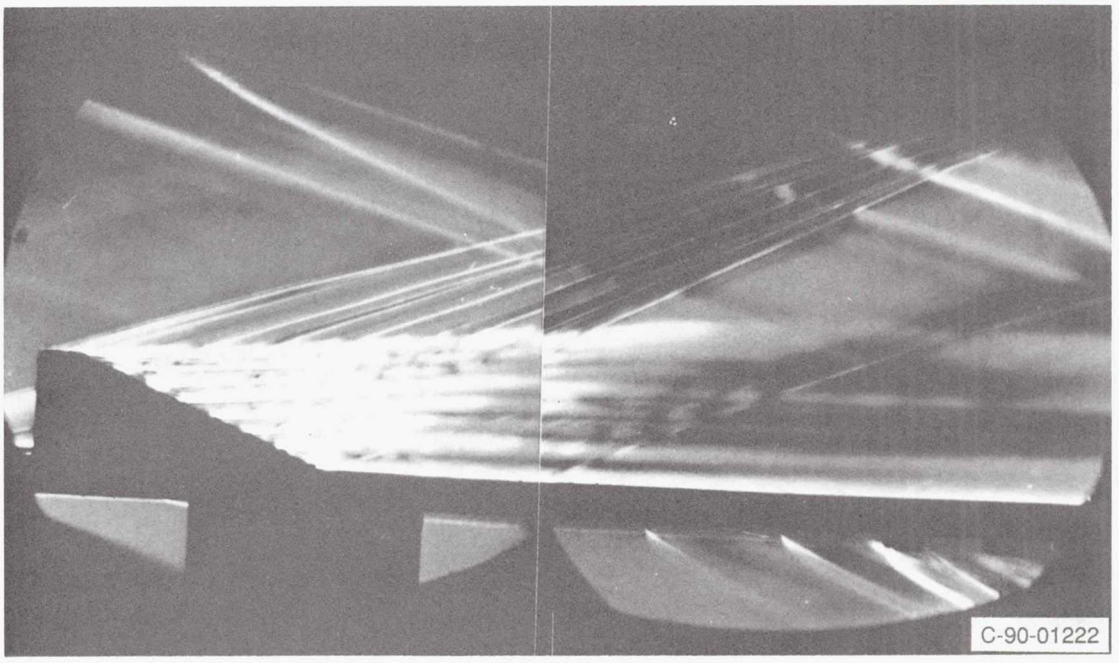

Figure 8.—Composite schlieren photograph of isolated honeycomb boundary layer simulator in two positions at Mach 4.0.

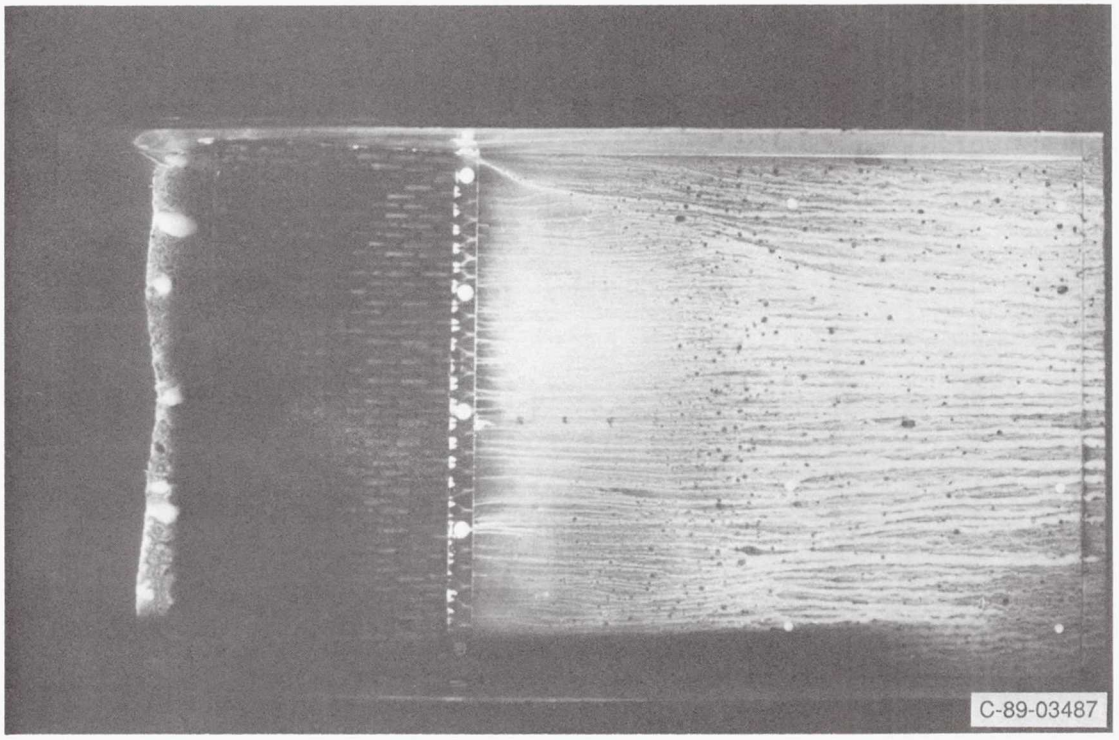

Figure 9.—Surface oil flow visualization results of NASA Lewis/Langley channel flow model at Mach 6.0 ($Re = 13.1 \times 10^6$/m).

This result is typical of what is seen in both channel flow models with the cowl at a 0° angle of attack, except that indications of upstream flow separation are not seen at the lower Mach numbers.

Figure 10 shows the results of surface oil flow visualization for the NASA Lewis channel flow model with an oblique-shock—simulated-boundary-layer interaction and an oblique-shock—naturally-occurring-boundary-layer interaction. In both cases, the tunnel free-stream nominal Mach number is 3.5, and the cowl wedge angle is 4°. The boundary layer edge Mach number is lower for the simulated boundary layer because of losses caused by the flow mixing process behind the boundary layer simulator. Again, the view is looking from above, and the flow proceeds from left to right. The cowl is removed so that the surface oil flow patterns in the channel can be seen. In figure 10(a), the oil flow results are for the simulated boundary layer. The results show the shock intersecting the model floor with no indication of large-scale boundary layer separation. Some curvature of the shock is indicated. This is most noticeable near the sidewalls, where the corner flow affects the interaction. For the same nominal free-stream Mach number and wedge angle, the oil flow results are shown in figure 10(b) for the case when the naturally occurring thick boundary layer is ingested into the channel. The results of the flow visualization show the shock intersection on the model floor with a curvature that is somewhat less pronounced than in the simulated boundary layer case. However, the general overall features of the flow do not differ between the two different boundary layers.

When the shock generator wedge angle is increased to 6°, the surface oil flow visualization results for the shock—boundary-layer interaction indicate that a large flow separation occurs on the model floor. These results are shown in figure 11 for both the simulated and the naturally occurring boundary layer. In each case, the upstream extent of the separation is not well defined, which is probably a result of large-scale unsteadiness. The flow unsteadiness was substantiated by the schlieren flow visualization, which indicated unsteadiness in the forward part of the model. The presence of the separation resulted in no direct indication of the shock intersecting the model floor. The general overall features for both the simulated and the naturally occurring boundary layer flows are the same. However, the separation region for the naturally occurring boundary layer case extends farther upstream.

Quantitative Results

The quantitative results of this investigation are wall static pressure measurements and flow-field surveys. Both kinds of measurements were made in all model configurations. The centerline streamwise static pressures were used as an aid to monitor the starting characteristics of the models during testing. In addition, they were used to document the boundary layer development on the flat plate or the channel floor. The effects of an oblique-shock—boundary-layer interaction also can be quantified by the centerline wall static pressure distribution.

Flow-field surveys included pitot and static pressure measurements and hot-wire measurements made at various axial locations in the models. These surveys were used to assess the development of the simulated boundary layer. For the isolated boundary layer simulator model, transverse pitot pressure profiles and hot-wire turbulence measurements were used to document the development of the simulated boundary layer. In the case of the channel flows, cross-plane rake pressure measurements were used to quantify the complex flow field, which contained thin developing sidewall boundary layers which interacted with the thick model floor boundary layer.

Surface Static Pressure Measurements

Isolated boundary layer simulator model.—The first set of wall static pressure data presented is for the isolated honeycomb boundary layer simulator model. These results are shown in figure 12 for a nominal free-stream Mach number of 4.0. In all cases, the wall static pressures are nondimensionalized by an upstream reference tunnel static pressure ($p/p_{s,u}$) and are plotted versus the number of cell diameters downstream of the boundary layer simulator ($x/D_{h/c}$). The reference static pressures for all test conditions are listed in table I.

For a boundary layer simulator height of 4.06 cm, the wall static pressure profiles exhibit similar trends for both the contoured and linear taper cross section. Up to a distance of 24 cell diameters downstream of the boundary layer simulator, the wall static pressures are approximately 10 percent higher than the reference free-stream tunnel static pressure. The static pressure distribution then decreases to a minimum and then begins to rise. The initial pressure rise may be the result of flow blockage induced by the presence of the boundary layer simulator. We believe that the waviness in the static pressure distribution is due to the flow mixing process behind the boundary layer simulator and the three-dimensional edge effects emanating from the sides of the boundary layer simulator since it does not completely span the tunnel.

When the height of the boundary layer simulator is increased to 6.35 cm, the static pressure distribution waviness becomes more apparent, as shown in the third plot in figure 12. It appears that the three-dimensional effects are more pronounced, and the increased height induces more flow blockage, as seen by the increased static pressure rise immediately behind the boundary layer simulator. In this figure, static pressure data are presented only to a distance of 60 cell diameters downstream of the boundary layer simulator. Downstream of this location, the simulated boundary layer flow is distorted by shock waves emanating from the boundary layer simulator that coalesce and reflect from the wind tunnel ceiling. Figure 8 shows a schlieren representation of this shock system.

NASA Lewis channel flow model.—The next series of wall static pressure distributions is presented in figure 13 for the NASA Lewis channel flow model. Results are shown for nominal Mach numbers of 3.0, 3.5, and 4.0. For a 0° cowl angle, surface static pressures are shown for both the simulated

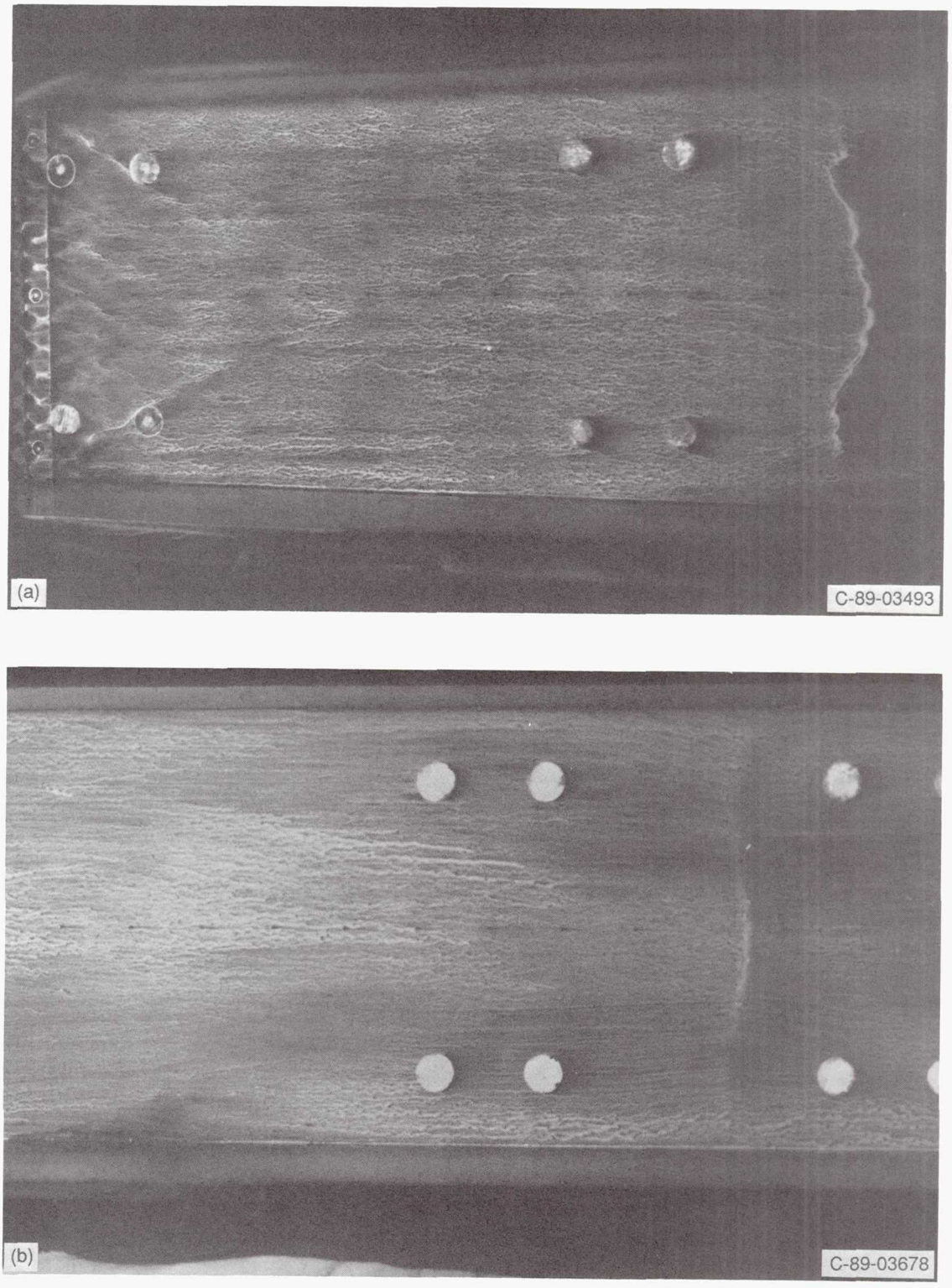

(a) Simulated boundary layer.
(b) Naturally occurring boundary layer.

Figure 10.—Surface oil flow visualization results of NASA Lewis channel flow model with oblique-shock—boundary-layer interaction at Mach 3.5 and cowl wedge angle of 4°.

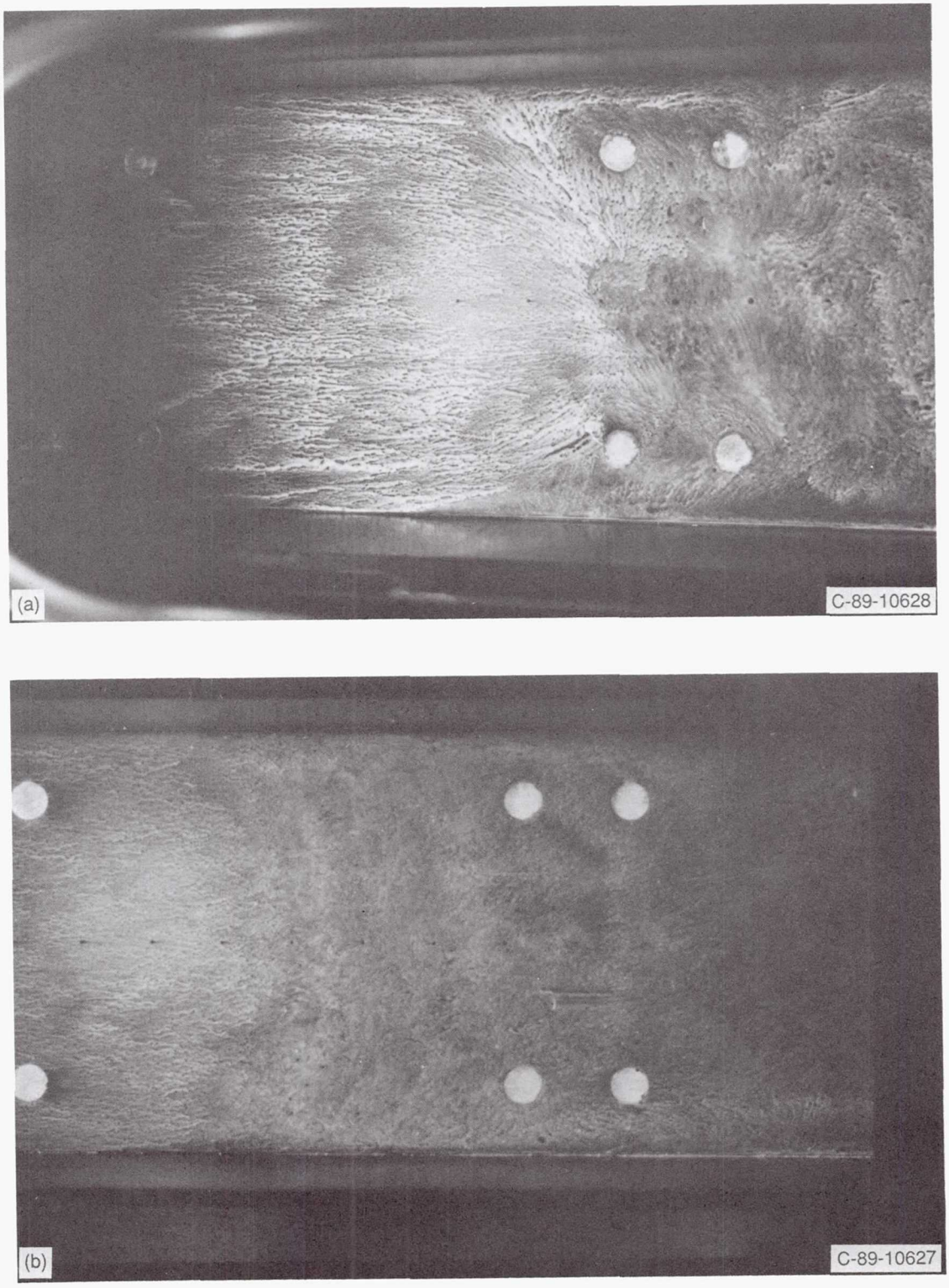

(a) Simulated boundary layer.
(b) Naturally occurring boundary layer.

Figure 11.—Surface oil flow visualization results of NASA Lewis channel flow model oblique-shock—boundary-layer interaction at Mach 3.5 and cowl wedge angle of 6°.

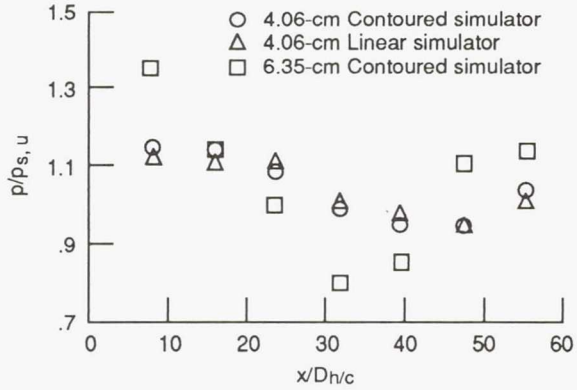

Figure 12.—Centerline static pressure distribution of isolated boundary layer simulator model at Mach 4.0.

and naturally occurring tunnel wall boundary layers. As mentioned previously, this configuration has the provision to be mounted in the tunnel free-stream, where the boundary layer simulator is used to generate an artificially thickened boundary layer in the channel. This model also can be relocated with the boundary layer simulator removed so that the naturally occurring tunnel sidewall boundary layers are ingested into the channel, thereby providing a comparison between the two cases. The boundary layer simulator is 4.06 cm high (53.3 percent of channel height), whereas the naturally occurring boundary layer is nominally 3 cm thick at the entrance to the channel.

The channel streamwise static pressure distributions show similar trends for both the simulated and naturally occurring boundary layers. The best agreement is at a nominal free-stream Mach number of 4.0. In all cases, a static pressure rise is seen from a Mach line that emanates from the cowl leading edge located 30 cell diameters downstream of the honeycomb boundary layer simulator. The Mach line occurs because of flow angularity in the channel caused by the floor boundary layer thickening.

The results of a shock wave interacting with the simulated boundary layer are presented for the Mach 3.5 and 4.0 cases. The cowl wedge angle is 4°, and in each case, the static pressure rise agrees well with the inviscid estimate that considers a cowl angle of 4°.

NASA Lewis/Langley channel flow model.—The centerline surface static pressure distributions for the Mach 6 channel flow model are shown in figure 14. Figures 14(a) and (b) show the static pressure distributions for the 43 and 57 percent of channel height boundary layer simulators, respectively. Since all cases in this experiment are conducted at a nominal Mach number of 6.0, the three sets of data per plot correspond to different Reynolds numbers test conditions.

The results indicate a slight Reynolds number variation, although the trends in the data are the same. As seen in the isolated boundary layer simulator results, the increased height induces a higher static pressure rise immediately behind the boundary layer simulator which then quickly recovers to a

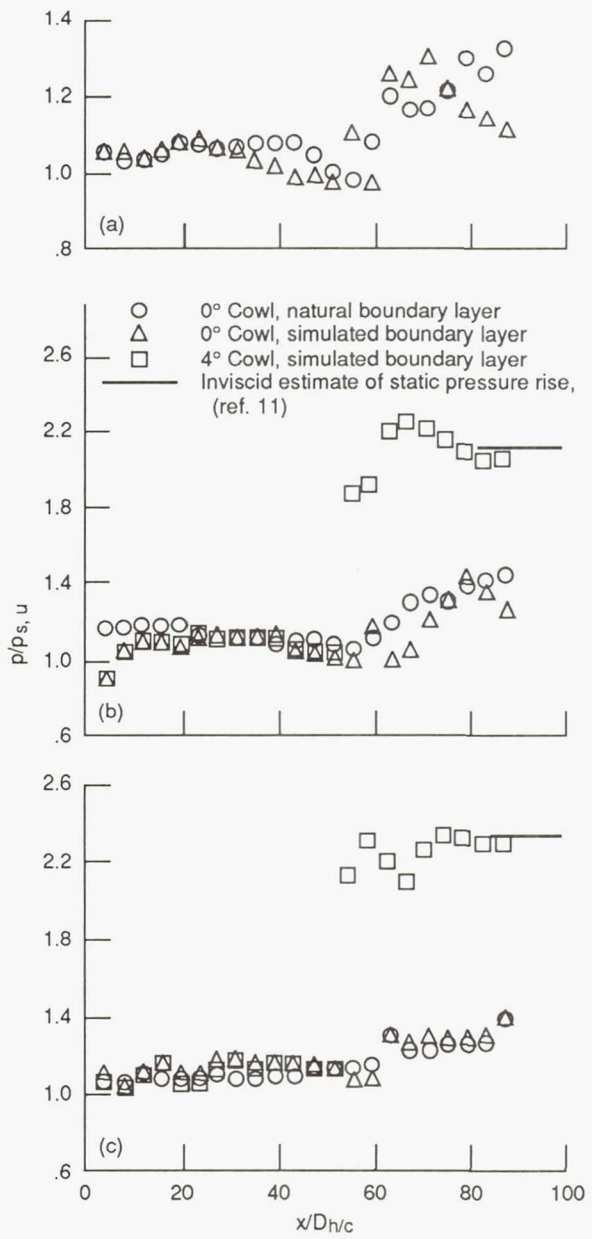

(a) Mach 3.0.
(b) Mach 3.5.
(c) Mach 4.0.

Figure 13.—Centerline static pressure distribution of NASA Lewis channel flow model at various free-stream Mach numbers.

static pressure distribution similar to the reduced-height boundary layer simulator. Again, we believe that the increased frontal area of the larger boundary layer simulator produces more flow blockage and a higher static pressure distribution immediately downstream.

For the two cases, after the initial static pressure rise, the streamwise static pressure distribution rises to a secondary maximum approximately 50 cell diameters downstream of the boundary layer simulator and then steadily decreases to the end of the channel. This trend is contrary to what is seen in

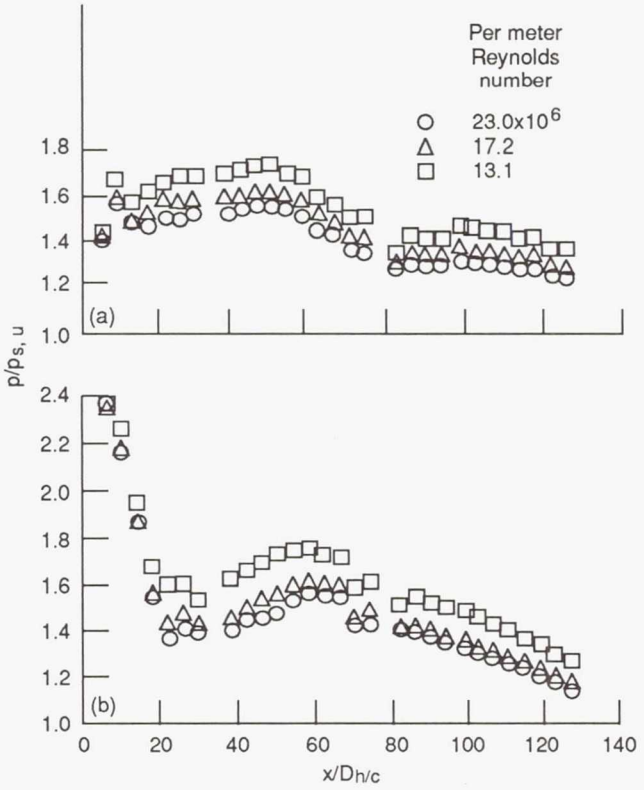

(a) 43-Percent channel height boundary layer simulator.
(b) 57-Percent channel height boundary layer simulator.

Figure 14.—Centerline static pressure distribution of NASA Lewis/Langley channel flow model at Mach 6.0.

a Fanno line process in which the streamwise static pressures increase as the flow tends to decelerate toward Mach 1. However, in this configuration, the cowl covers only the last 20 percent of the model; this region is the only section that can be considered as flow in a constant-area channel. Apparently, the flow-field mixing process behind the boundary layer simulator induces a favorable streamwise pressure gradient in the rear portion of the channel. The static pressure distributions in the NASA Lewis channel model which was tested at lower Mach numbers did not exhibit this behavior.

Flow-Field Measurements

Isolated boundary layer simulator model.—The first phase of this investigation primarily was aimed at determining the feasibility of the simulated boundary layer concept. Therefore, the isolated boundary layer simulator model was chosen as the initial test article. Flow-field measurements in the form of centerline pitot pressure and hot-wire anemometry were made. Transverse pitot pressure surveys were conducted at numerous streamwise positions downstream of the boundary layer simulator in order to document the simulated boundary layer development. In addition, hot-wire measurements were made for both the simulated boundary layer and naturally occurring tunnel sidewall boundary layer in order to compare the corresponding turbulence levels. For these series of results, the nondimensional pitot pressures (P_t/P_o) were plotted versus the nondimensional boundary layer height (y/δ). In the case of the artificially generated boundary layer, the boundary layer height nondimensionalizing variable $\delta_{h/c}$ was chosen as being the physical height of the boundary layer simulator.

Figure 15 shows the streamwise simulated boundary layer development at the isolated model centerline as the flow proceeds from a distance of 13.5 to approximately 50 cell diameters downstream of the boundary layer simulator. These

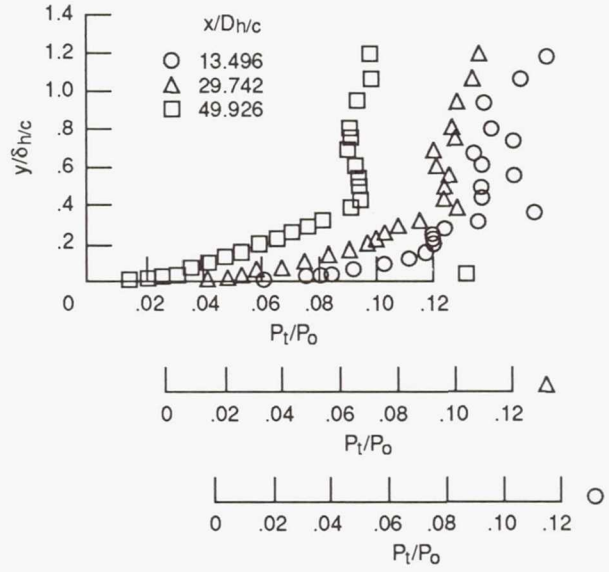

Figure 15.—Centerline streamwise pitot pressure profiles of isolated boundary layer simulator model at Mach 4.0 ($\delta_{h/c}$ = 4.06 cm).

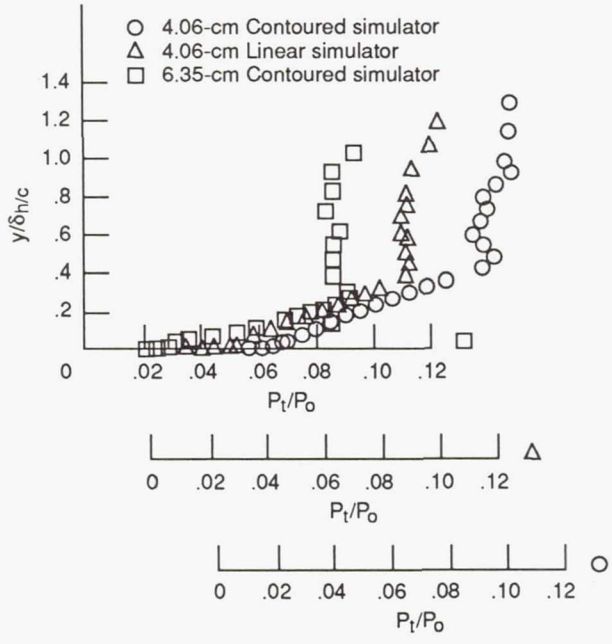

Figure 16.—Centerline pitot profiles of isolated boundary layer simulator model at Mach 4.0 ($x/D_{h/c}$ = 46).

results are for the 4.06-cm linear contour at a tunnel free-stream nominal Mach number of 4.0. The simulated boundary layer mixing process clearly can be seen. Initially, the pitot pressure profiles are discontinuous, but as the flow proceeds downstream, the profiles smooth out, forming the characteristic profile of a turbulent boundary layer.

Selected pitot profiles at an axial measurement location 46 cell diameters downstream of the boundary layer simulator for the two heights and honeycomb contours are shown in figure 16. In all cases, the free-stream nominal tunnel Mach number is 4.0. Even though the cross-sectional shapes of the two 4.06-cm boundary layer simulators are different, the pitot profiles are similar, especially in the lower third of the boundary layer. However, when the contoured boundary layer simulator height is increased to 6.35 cm, the resulting profile shows a lower total pressure loss trend in the lower third of the boundary layer. This difference could be a result of the increased blockage due to the larger honeycomb size. The apparent blockage effects were seen in the surface static pressure measurements presented earlier.

Pitot pressure profiles for the 4.06-cm linear contoured boundary layer simulator for free-stream nominal Mach numbers of 3.5 and 4.0 are shown in figure 17. For each Mach number, pitot pressure profiles are plotted at measurement locations 46 and 50 cell diameters downstream of the boundary layer simulator. The upper half of the flow field generated by the simulator appears to yield a relatively constant Mach number region for the Mach 4.0 case, as evidenced by the flatness of the pitot pressure profile. However, the Mach 3.5 results indicate that the shock wave system generated by the boundary layer simulator reflects from the wind tunnel ceiling and distorts the pitot pressure profiles. Refer to figure 8 for a typical schlieren photograph of this shock system. At 46 cell diameters downstream of the boundary layer simulator, the reflected shock passes through the survey station at approximately 90 percent of the boundary layer simulator height. At the rear survey location, the effects of the reflected shock become more pronounced, as shown by the distortion of the pitot pressure profile at 50 percent of boundary layer simulator height.

Taking the pitot profiles of figure 17 into consideration, an effective boundary layer δ_{eff} height was chosen based on the approximate location where the pitot pressure profile flattens. For the nominal Mach number of 4.0, δ_{eff} was found to be 1.78 cm (44 percent of boundary layer simulator height). Using this value, the pitot profile was analyzed by a wall-wake curvefit for a turbulent compressible boundary layer described in reference 7. These results are shown in figure 18. In this figure, the measurements are transformed into a nondimensional velocity profile by the wall-wake analysis. The symbols represent the experimental data, and the solid line is the wall-wake curvefit results. This shows that the boundary layer simulator does indeed produce a boundary layer that duplicates the momentum profile of a naturally occurring turbulent boundary layer. However, the generated boundary layer is not

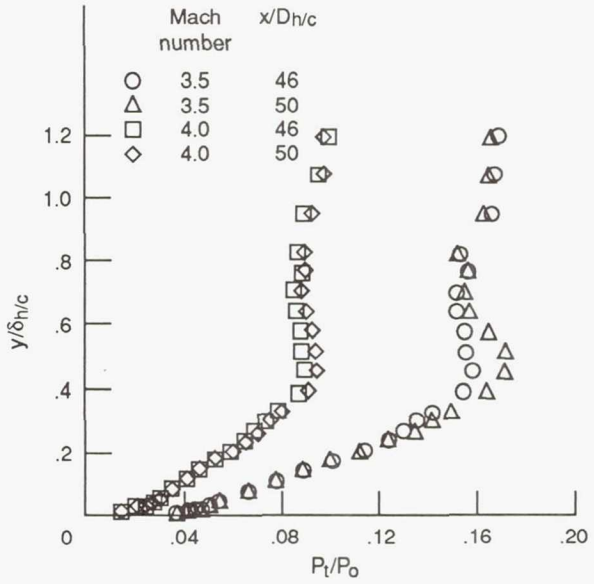

Figure 17.—Centerline pitot profiles of linear-contoured isolated boundary layer simulator model.

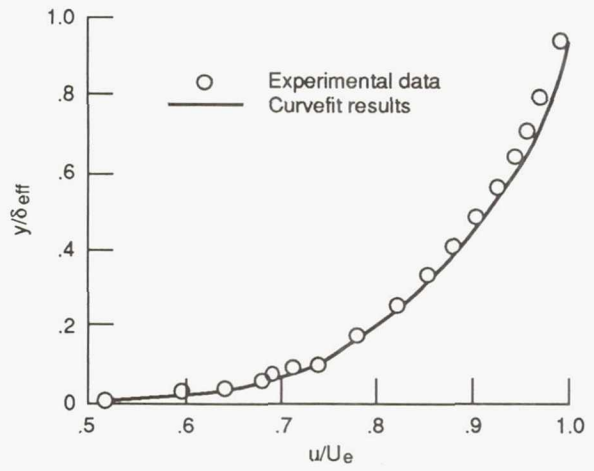

Figure 18.—Simulated boundary layer wall-wake curvefit results at Mach 4.0 ($x/D_{h/c} = 50$).

as thick as the boundary layer simulator height, which indicates that the upper portion of the boundary layer simulator is ineffective in the momentum removal process.

We feel that there are two factors that contribute to the inability of the boundary layer simulator to generate an artificially thickened boundary layer that spans the full simulator height. First, we must consider the design of the boundary layer simulator. Initially, the transverse contour of the boundary layer simulator was determined by assuming that the flow through each honeycomb cell follows a Fanno line process. That is, the length of each honeycomb cell was tailored by a Fanno line analysis to achieve an exit Mach number that would be found in a one-seventh power law turbulent boundary layer profile. The Fanno line analysis assumed that the flow was turbulent throughout the entire cell length, and the empirical

relation for skin friction found in reference 8 was used to determine the skin friction coefficient.

The resulting cell lengths of the boundary layer simulator shorten from the model floor to the free-stream. As the cell lengths shorten, the flow through these cells tends to be increasingly laminar rather than turbulent. Therefore, the turbulent flow assumption for the Fanno line analysis in this region underestimates the cell length needed to match the specified exit Mach number at that transverse location, and this section of the boundary layer simulator becomes ineffective.

The second and dominant mechanism contributing to the ineffectiveness of the boundary layer simulator's upper region are the increasing shock losses in the transverse direction. Referring to the schlieren photographs of figures 7 and 8, a compression fan can be seen at the exit of the boundary layer simulator which is composed of a series of compression waves that emanate from each transverse cell mixing layer boundary. Towards the upper edge of the boundary layer simulator, the exiting flow passes through an increasing number of these compression waves which causes higher total pressure losses.

One of the objectives of this experiment was to evaluate the turbulence level of the simulated boundary layer as well as to measure the momentum distribution. In preparation of this effort, turbulence measurements were made of the naturally occurring boundary layers on the wind tunnel sidewall in order to obtain a baseline comparison with the simulated boundary layer turbulence measurements. Figure 19 depicts the results of these measurements for a nominal free-stream Mach number of 3.5. They are plotted so that a direct comparison between data taken at different test conditions can be made. The expression $(\rho/\rho_w)^{1/2}\ (u'/u_\tau)$ is the nondimensional axial component of turbulence. The thickness of the naturally occurring boundary layer is approximately 2.65 cm. The friction velocity is obtained from a wall-wake curvefit of the corresponding pitot pressure profile (ref.7). The figure shows that the naturally occurring boundary layer results are in good agreement with earlier measurements (refs. 9 and 10).

The results of the axial turbulence measurements for the simulated boundary layer are shown in figure 20. The free-stream nominal Mach number is 3.5, and the measurements are made 64 cell diameters downstream of the boundary layer simulator. As in figure 19, the data are plotted by using nondimensional variables. These results show that the turbulence levels of the simulated boundary layer are substantially lower than what would be expected from a naturally occurring boundary layer. At approximately half span of the boundary layer simulator, the turbulence levels become negligible. This is an indicator that the momentum profile in this region has reached a relatively constant "free-stream" value which previously was documented by the flatness of the centerline pitot pressure profiles in this region.

NASA Lewis channel flow model.—The next series of flowfield survey results presented are cross-plane Mach number contours for the Lewis channel flow model. The actual experimental data are sequential rake pitot and static pressure surveys taken at various axial cross planes. Therefore, for a constant test condition (i.e., same model geometry, free-stream Mach number, and Reynolds number), the corresponding cross-plane pitot and static pressure datasets are used to create a Mach number contour dataset. The Rayleigh pitot formula found in reference 11 is used to relate the local pitot and static pressures to a local Mach number. For these series of contour plots, the spanwise coordinate z is nondimensionalized by the model span width S (15.24 cm). The channel height coordinate y is nondimensionalized by the channel height H (7.62 cm).

The Lewis channel flow model was tested at nominal Mach numbers of 3.0, 3.5, and 4.0 with two cowl angles of 0° and 4°. The removable honeycomb boundary layer simulator spans 53 percent of the channel height. For the Mach 3.5 and 4.0 conditions, the following cross-plane Mach number contour results are presented: (1) cowl exit survey for 0° cowl and ingestion of naturally occurring tunnel wall boundary layer (case 1), (2) cowl entrance survey located 30 cell diameters downstream of the boundary layer simulator (case 2), (3) cowl

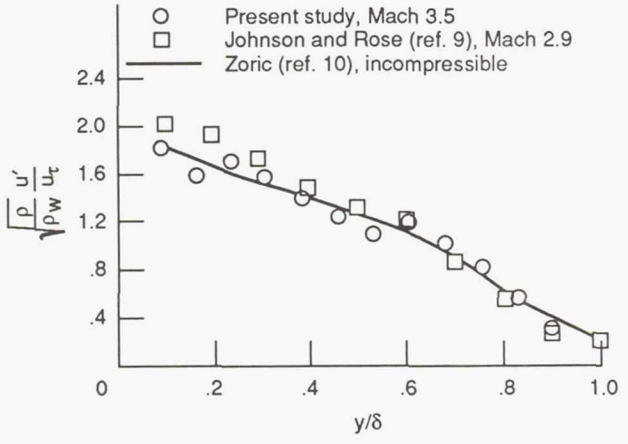

Figure 19.—Naturally occurring boundary layer axial turbulence profile at Mach 3.5.

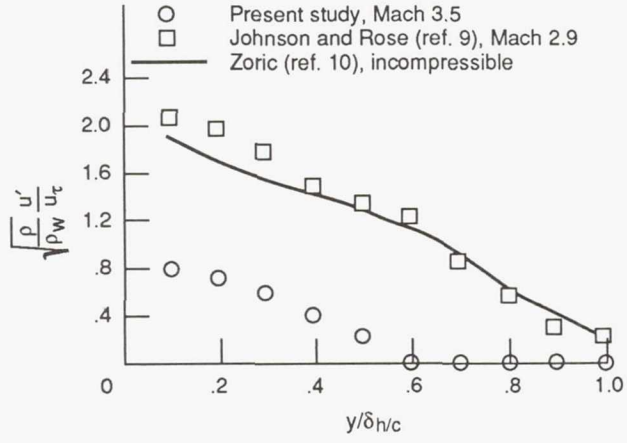

Figure 20.—Simulated boundary layer axial turbulence profile at Mach 3.5.

exit survey for 0° cowl located 88 cell diameters downstream of boundary layer simulator (case 3), and (4) cowl exit survey for the 4° cowl (case 4). Cases 2 to 4 have the boundary layer simulator installed. The Mach 3.0 results include cases 1 and 3 only. For clarity, a side view schematic of the channel model and the survey locations are shown in figure 21.

The first results are presented for the cowl exit flow-field survey of the ingested naturally occurring tunnel wall boundary layer, case 1. The tunnel free-stream nominal Mach number is 3.0. The cross-plane Mach number contours shown in figure 22(a) reveal that the ingested boundary layer is well behaved and that it has grown to approximately 40 percent of the channel height. The concavity of the Mach number contours in the corner regions of the channel show the effects of the ingested boundary layer interaction with the thin, developing channel sidewall boundary layers. The results also indicate a well-defined core flow region in the channel.

Figure 22(b) shows the Mach 3.0 cowl exit survey results for the ingested simulated boundary layer, case 3. The Mach number contours show transverse gradients characteristic of boundary layer development near the model floor. In this case, the gradient region is thin, about 20 percent of the channel height with an edge Mach number of 2.25. Next, a transverse gradient region is found where the Mach number distribution gradually increases to 2.50 at 60 percent of the channel height, which is the approximate location of the upper edge of the boundary layer simulator. The upper portion of the boundary layer simulator appears to be ineffective in tailoring the momentum profile. At the top of the channel, just beneath the cowl and above the boundary layer simulator, there is another

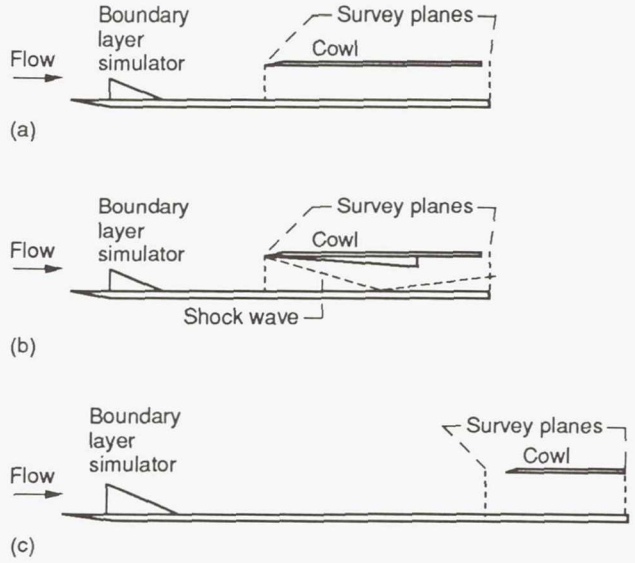

(a) Lewis channel flow model with cowl angle of 0°.
(b) Lewis channel flow model with cowl angle of 4°.
(c) Lewis/Langley channel flow model.

Figure 21.—Schematic of channel flow model survey locations.

transverse gradient region in the flow-field that approaches the free-stream Mach number of 3.0. An overall comparison of this plot with that of the ingested naturally occurring boundary layer, figure 22(a), shows that essential flow physics such as the concavity of the Mach number contours in the channel corner regions are retained. However, inspection of the Mach number contours at this survey plane shows that the flow is still adjusting to the sudden momentum loss due to the artificial boundary layer generation process, as evidenced by the waviness of the Mach number contours.

The next series of channel cross-plane Mach number contours are presented for a tunnel nominal free-stream Mach number of 3.5. The cowl exit survey results for the ingested naturally occurring wind tunnel boundary layer, case 1, are shown in figure 23(a). Again, the ingested boundary layer has grown to 40 percent of the channel height, and a well-defined core flow region has developed.

Figure 23(b) shows the upstream cowl entrance flow-field survey results with the boundary layer simulator installed, case 2. Because of geometrical constraints of the probe actuation system, only 4.95 cm on either side of the model centerline could be surveyed at this axial plane. Therefore, the Mach number contours do not show the effect of the simulated boundary layer interacting with the channel sidewall boundary layers. Here the boundary layer gradient region is quite thin, about 15 percent of the channel height, with an edge Mach number approaching 2.65. At the edge of the boundary layer gradient, another transverse gradient region is found where the Mach number distribution increases to a Mach number of 3.0 at 70 percent of the channel height just above the upper edge of the boundary layer simulator. Near the top of the channel, just beneath the cowl and above the boundary layer simulator, there is a gradient region in the flow field that approaches the wind tunnel free-stream nominal Mach number of 3.5.

As the flow proceeds through the channel, the simulated boundary layer thickens, which is typical of developing channel flow. At the exit of the channel, the steep Mach number gradient region has grown to approximately 25 percent of the channel height with a lesser gradient region approaching midchannel height. At the edge of the boundary layer gradient region, the Mach number approaches 2.50 with a gradual increase to a Mach number of 2.75 at midchannel height. The overall Mach number contours shown in figure 23(c) tend to be lower relative to the results shown at the cowl entrance, which indicates that the flow is decelerating through the channel. The Mach number distribution is more uniform at this cross plane than at the upstream survey plane. This indicates that the flow adjustment process due to the upstream momentum defect is proceeding well. In addition, this survey location captures the effects of the thin sidewall boundary layers interacting with the thick channel floor simulated boundary layer.

The effects of an oblique-shock—simulated-boundary-layer interaction for a free-stream Mach number of 3.5 are shown

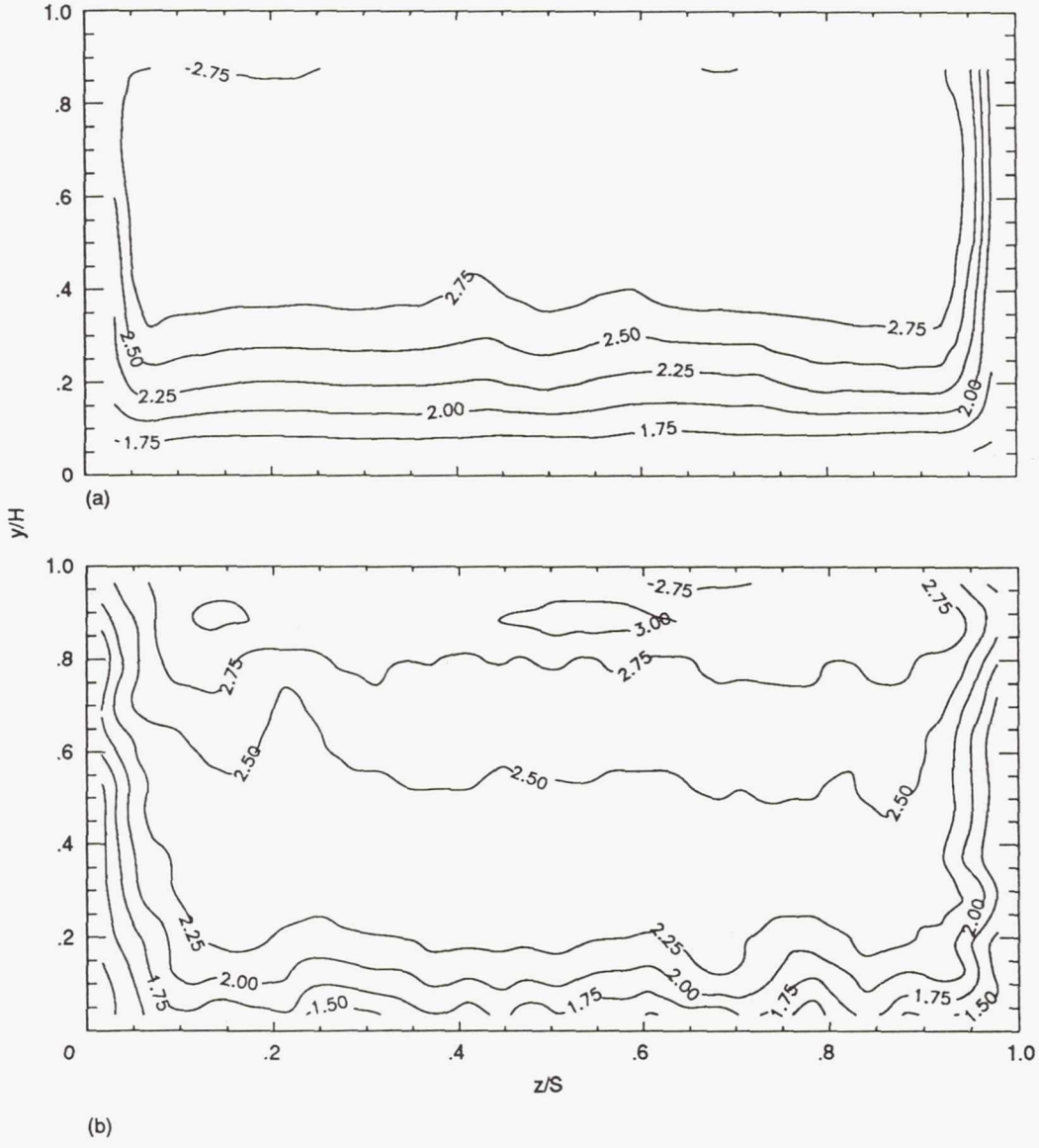

(a) Naturally occurring boundary layer.
(b) Simulated boundary layer.

Figure 22.—Cross-plane Mach number contours for Lewis channel flow model at Mach 3.0 with cowl angle of 0° (cowl exit survey).

in figure 23(d). The cowl wedge angle is 4°, and the survey location is at the cowl exit. Referring to the schematic in figure 21, the incident shock wave impinges on the simulated boundary layer upstream of the survey plane, and the reflected shock passes through the survey location. Also, since the cowl wedge does not extend past the survey plane, an expansion wave emanates from the wedge trailing edge and passes through the survey plane. The expansion wave effects can be seen clearly as the severe transverse Mach number gradient at the upper portion of the survey plane. Below the interaction region, the results of the oblique-shock—simulated-boundary-layer interaction are seen. Comparison of these Mach number contours to the contours of the no-shock case, fig. 23(c), shows that the impinging shock thickens and distorts the simulated boundary layer, especially in the corner regions. The overall Mach number levels seen in the area influenced by the reflected shock are lower than for the no-shock case.

An inviscid analysis was used to determine the approximate location of the reflected shock wave and the lower bounds of the expansion fan which emanates from the cowl trailing edge. These estimated locations are shown in figure 23(d). The analysis predicts that the expansion fan intersects the reflected shock wave.

The flow-field survey results for a nominal Mach number of 4.0 are shown in figure 24. The cowl exit cross-plane Mach number contours in figure 24(a) show that the ingested, naturally occurring, tunnel wall boundary layer has grown to approximately 45 percent of the channel height. A core flow region is present, but it is not as well defined as in the Mach 3.0 and 3.5 results. However, the results do indicate

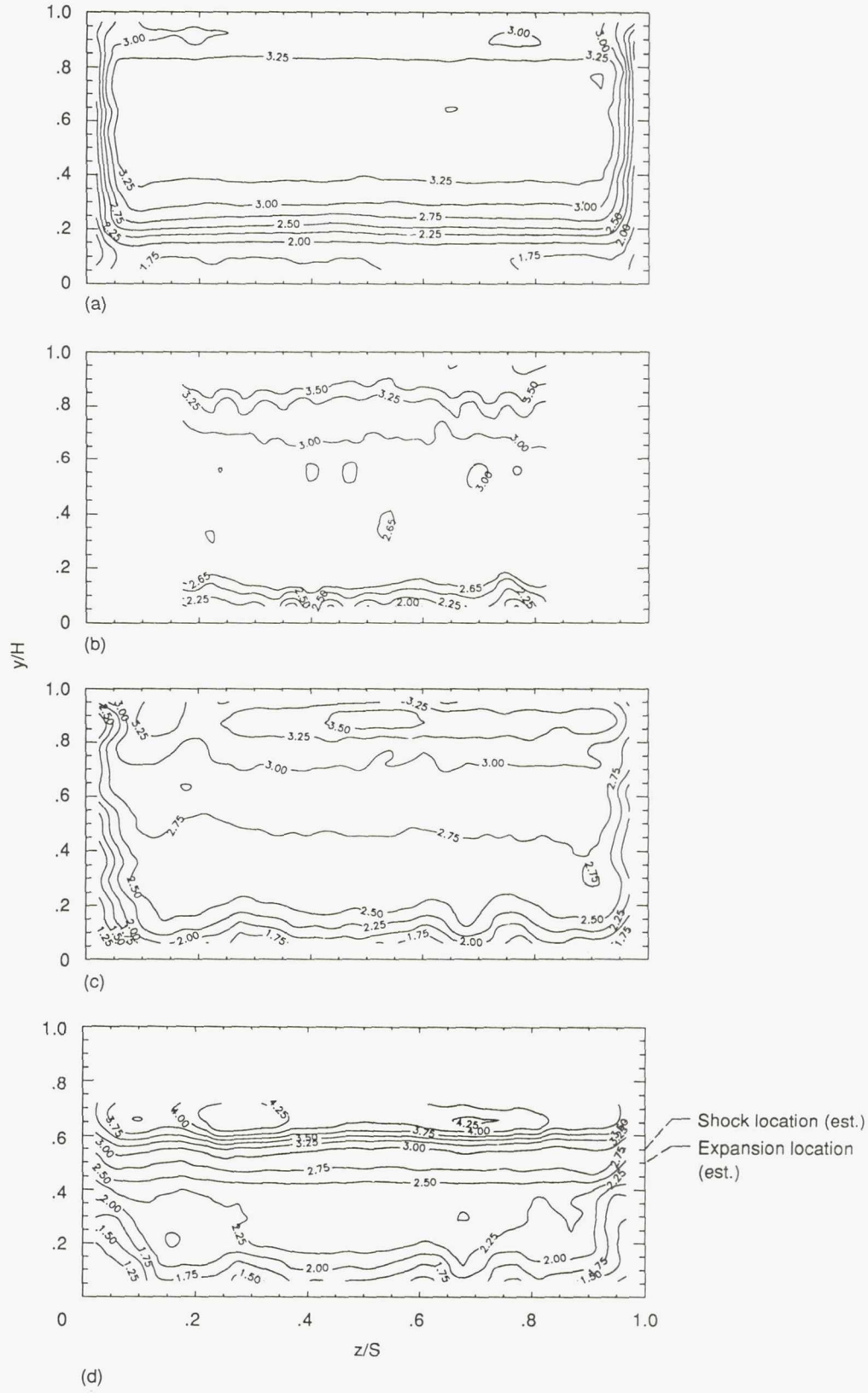

(a) 0° Cowl angle, naturally occurring boundary layer (cowl exit survey).
(b) 0° Cowl angle, simulated boundary layer (cowl entrance survey).
(c) 0° Cowl angle, simulated boundary layer (cowl exit survey).
(d) 4° Cowl angle, simulated boundary layer (cowl exit survey).

Figure 23.—Cross-plane Mach number contours for Lewis channel flow model at Mach 3.5.

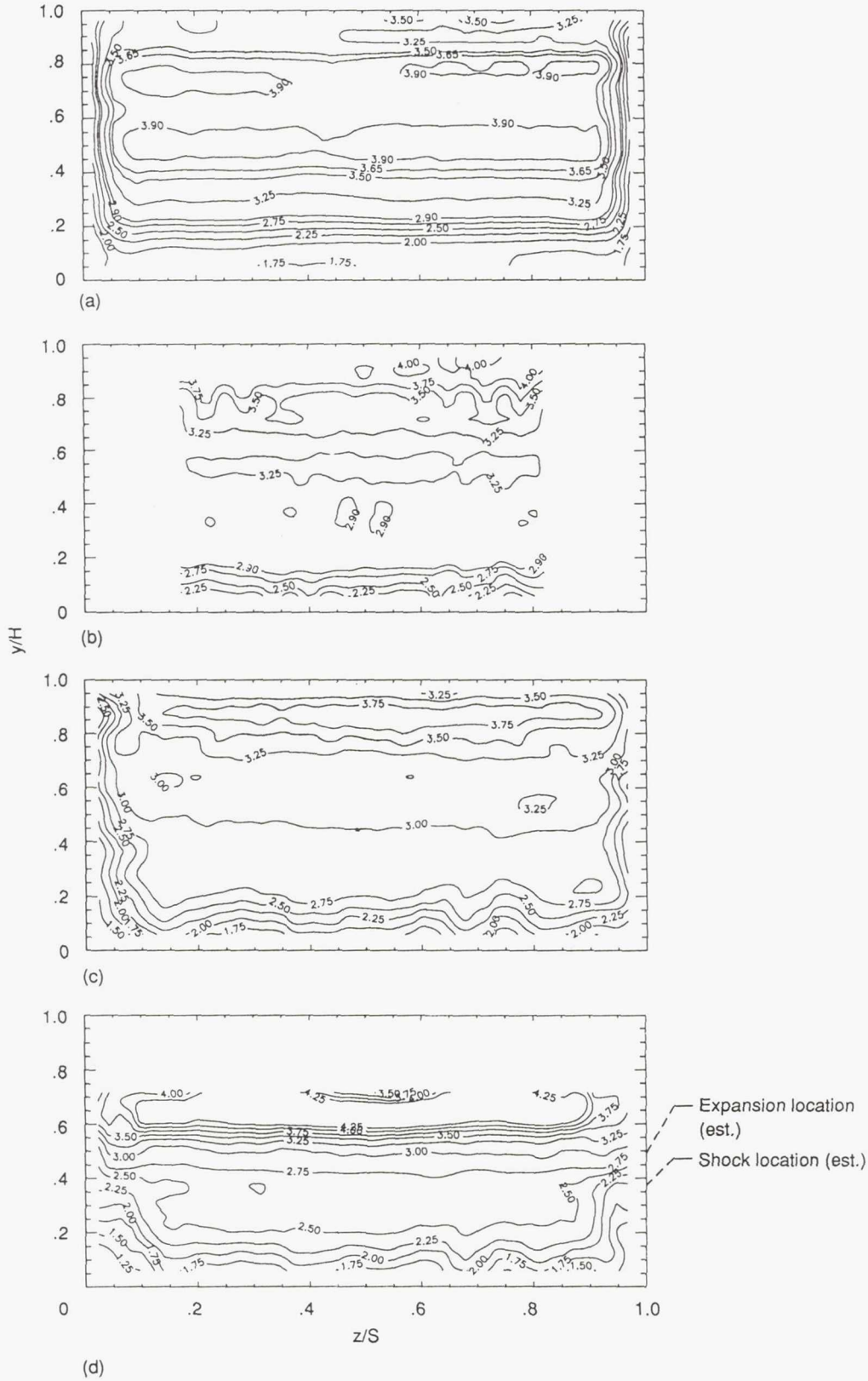

(a) 0° Cowl angle, naturally occurring boundary layer (cowl exit survey).
(b) 0° Cowl angle, simulated boundary layer (cowl entrance survey).
(c) 0° Cowl angle, simulated boundary layer (cowl exit survey).
(d) 4° Cowl angle, simulated boundary layer (cowl exit survey).

Figure 24.—Cross-plane Mach number contours for Lewis channel flow model at Mach 4.0.

a well-behaved flow field as evidenced by the uniformity of the Mach number contours near the channel floor and sidewalls.

The Mach number contours presented in figure 24(b) show the flow-field characteristics at the channel cowl entrance with the boundary layer simulator installed. The overall features of the flow field look similar to what is seen at Mach 3.5, although the transverse Mach number gradient at the top of the channel near the cowl surface is more pronounced.

Next, the cowl exit flow-field survey results for the artificially thickened boundary layer are shown in figure 24(c). Similar to the Mach 3.5 results, the overall Mach number levels are lower, and the channel floor boundary layer has thickened relative to the upstream cowl entrance survey. This trend is expected since supersonic flow in a constant area duct follows a Fanno line process which tends to decelerate the flow toward Mach 1.

The cowl exit survey results for the case when an oblique-shock—simulated-boundary-layer interaction generated by a 4° wedge at a wind tunnel nominal free-stream Mach number of 4.0 are shown in figure 24(d). The same simulated boundary layer distortion effects seen at Mach 3.5 are present. The estimated locations of the expansion fan and reflected shock wave are shown in the figure. Here the cowl expansion fan does not intersect the reflected shock. A comparison with the Mach 3.5 results indicates that the Mach number gradient caused by the expansion fan is more pronounced for the Mach 4.0 case.

Associated with the simulated boundary layer generation process are losses in the honeycomb that are shock dominated. Comparison of the core Mach numbers seen at the rear survey plane in the channel for the naturally occurring and simulated boundary layers tested at the same conditions shows that the naturally occurring boundary layer consistently has the higher core Mach number. The following approach is taken to quantify these losses.

First, the data at the 0° cowl exit survey plane are used for the loss calculation because at the same tunnel free-stream nominal Mach numbers tested, both naturally occurring and simulated boundary layer data exist (figs. 22 to 24). Next, the boundary layer edge Mach number is determined. In the case of the simulated boundary layer, the edge Mach number is chosen as being the Mach number near the physical edge of the boundary layer simulator, $M_{h/c}$. For the naturally occurring boundary layer, the edge Mach number is chosen in the region where the Mach number is relatively constant just above the boundary layer gradient, M_{nb}. In order to assess the efficiency of the boundary layer simulation technique, it is prudent to express this efficiency in terms of a percentage. Therefore, the ratio $M_{h/c}/M_{nb}$ is used to quantify the efficiency of the boundary layer simulator. This ratio is plotted versus the natural boundary layer edge Mach number M_{nb} because in an actual application of this loss estimate, the natural boundary layer edge Mach number would be the wind tunnel free-stream Mach number.

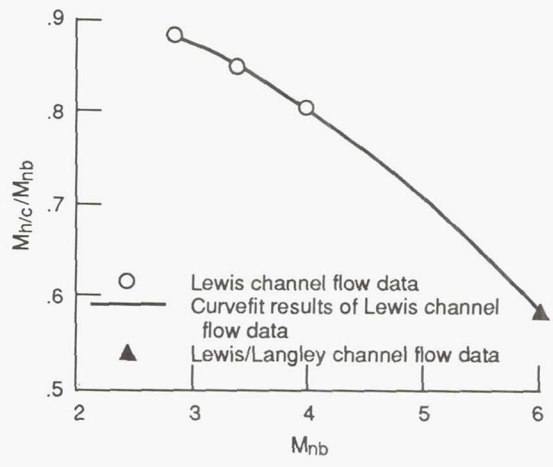

Figure 25.—Boundary layer simulator efficiency estimate.

This procedure was applied to the channel flow model, and the results are shown in figure 25. The efficiency $M_{h/c}/M_{nb}$ is plotted as the ordinate versus the natural boundary layer edge Mach number M_{nb}. It appears that a second order curvefit quantifies these results since the extrapolation of this curvefit to Mach 6 follows the loss trends seen in the Mach 6 channel flow model data which will be presented subsequently. The results for this honeycomb boundary simulator family (linear taper) indicate that as the free-stream tunnel operating Mach number increases, the boundary layer simulation technique becomes less efficient. At a tunnel free-stream Mach number of 3.0, the edge Mach number of the boundary layer simulator is approximately 2.6, or an efficiency of 87 percent. However, at Mach 4.0, the efficiency decreases to 80 percent. Use of this technique to generate an artificially thickened boundary layer does produce total pressure losses; this fact must be considered in subsequent applications.

NASA Lewis/Langley channel flow model.—The results for this portion of the investigation are presented as cross-plane Mach number contours determined from local pitot and static rake pressure measurements. Again, the plot coordinates are nondimensionalized by the channel dimensions ($S = 29.21$ cm, $H = 8.89$ cm). Two linear taper boundary layer simulators were used to generate the artificially thickened boundary layer. They corresponded to 43 and 57 percent of the channel height. Since all the testing was conducted at a nominal Mach number of 6.0, it is opportune to investigate Reynolds number effects during this experiment. Three unit Reynolds numbers were chosen: 13.1, 17.2, and 23.0×10^6/m. The first condition overlapped those of the testing conducted in the NASA Lewis 1- by 1-Foot SWT, while the last two conditions were chosen to exploit the higher Reynolds number capability of the NASA Langley 20-Inch—Mach 6 HWT. For each configuration, results are presented for two survey plane locations. The first survey plane was located 10 cell diameters upstream of the cowl leading edge, which is equivalent to 86 cell diameters downstream of the boundary layer simulator. Therefore, the

simulated boundary layer development was documented before entering the full channel. The other survey plane was located at the cowl exit, 126 cell diameters downstream of the boundary layer generator. Figure 21 shows these survey stations.

Cross-plane Mach number contours are shown in figure 26 for the 43-percent channel height boundary layer generator operating at a nominal Mach number of 6.0 and a unit Reynolds number of 23.0×10^6/m. Both survey planes show Mach number gradients characteristic of boundary layer development in the lower third of the channel. From this point up to the physical edge of the boundary layer simulator, there is little or no Mach number gradient. This trend was seen in both the isolated boundary layer simulator model and the Lewis channel flow model when tested at lower Mach numbers. From the physical edge of the boundary layer simulator to the cowl, another transverse Mach number gradient region was found. At the front survey plane, just upstream of the cowl, the local Mach number approaches 5.5 at the top of the channel, while at the cowl exit survey plane, the maximum Mach number in this gradient region has reduced to 4.5. A comparison of the front and rear axial plane Mach number contours shows that as the flow proceeds through the channel, the simulated boundary layer becomes well-behaved, as evidenced by the smoothness of the channel floor boundary layer contours at the cowl exit plane relative to the contours at the cowl entrance plane. When comparing the overall local Mach number distribution between the two channel locations, the flow decelerates.

Inspection of the data used to generate the cross-plane Mach number contour plots shows that the boundary layer simulator edge Mach number at the cowl entrance cross plane is about 3.75 and decreases to a Mach number of 3.50 at the cowl exit survey plane. These losses follow the trends of the Lewis channel flow model data shown in figure 25 which predicts that, at a nominal Mach number of 6.0, the honeycomb edge Mach number would be 3.53. This results in an efficiency of only 59 percent.

In figure 27, flow-field survey results are shown for the 57 percent of channel height boundary layer simulator, again operating at a nominal Mach number of 6.0 and a unit Reynolds number of 23.0 million/m. Even though the boundary layer simulator is larger, the artificially generated boundary layer is approximately the same height as the one produced by the reduced-height boundary layer simulator. As seen in previous results, there is a relatively constant Mach number region at the upper portion of the boundary layer simulator. The main difference seen in the flow field between the two configurations is that the Mach number gradients near the cowl are less pronounced for the larger boundary layer simulator.

Figures 28 through 31 depict the flow-field survey results for unit Reynolds numbers of 17.2 and 13.1 million/m operating at a nominal Mach number of 6.0. The physical features of the flow field at each cross plane are similar to those of the high Reynolds number cases previously discussed. The simulated boundary layer thicknesses do not vary significantly

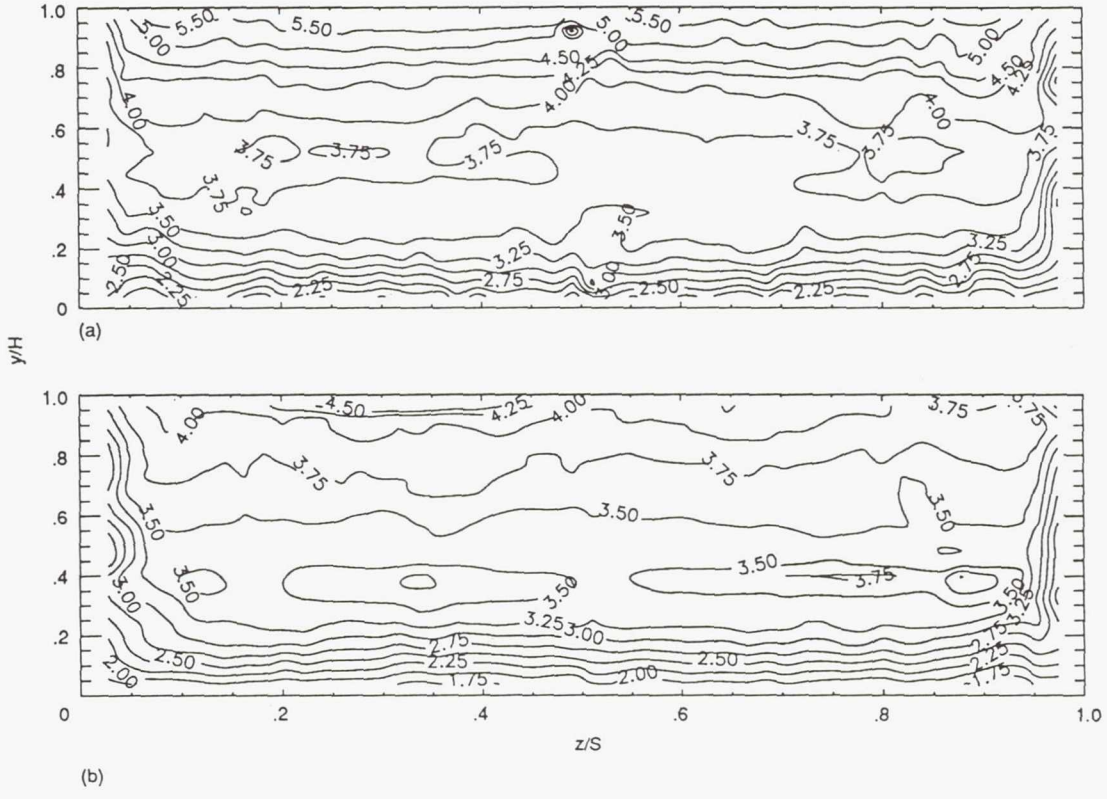

(a) Cowl entrance survey. (b) Cowl exit survey.

Figure 26.—Cross-plane Mach number contours for Lewis/Langley channel flow model at Mach 6.0, $\delta_{h/c}$ = 3.82 cm, and Re = 23.0×10^6/m.

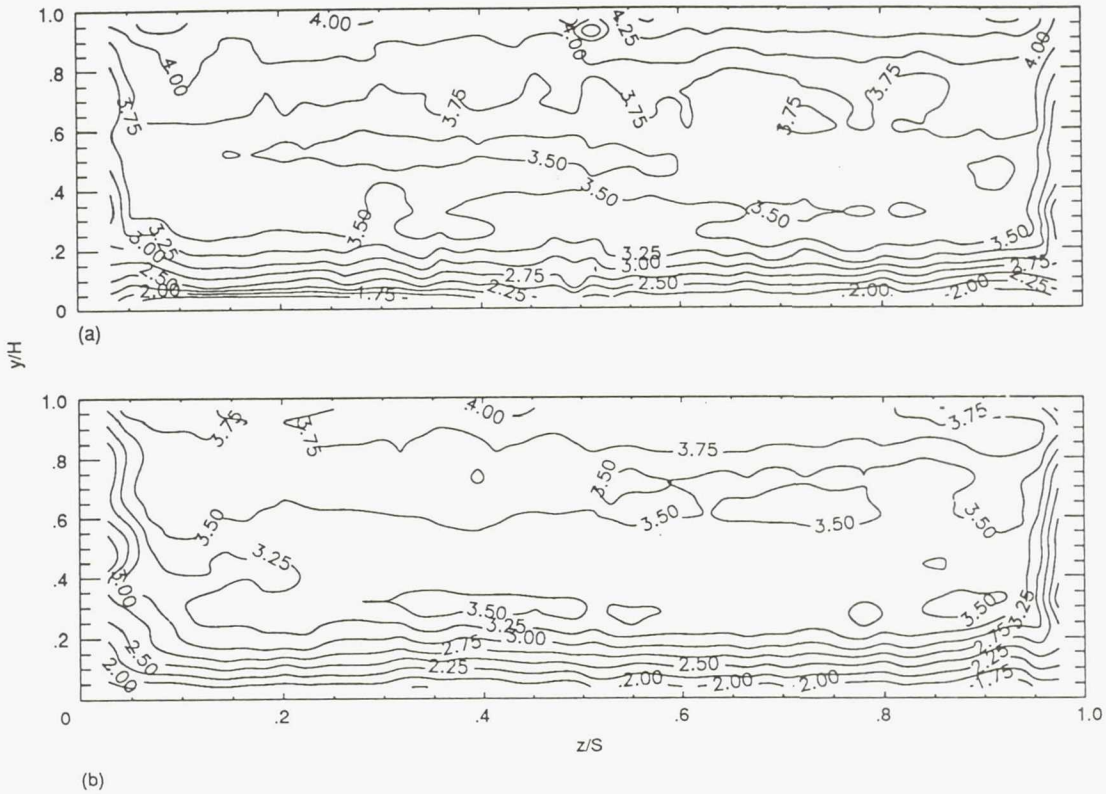

(a) Cowl entrance survey. (b) Cowl exit survey.

Figure 27.—Cross-plane Mach number contours for Lewis/Langley channel flow model at Mach 6.0, $\delta_{h/c}$ = 5.07 cm, and Re = 23.0×10^6/m.

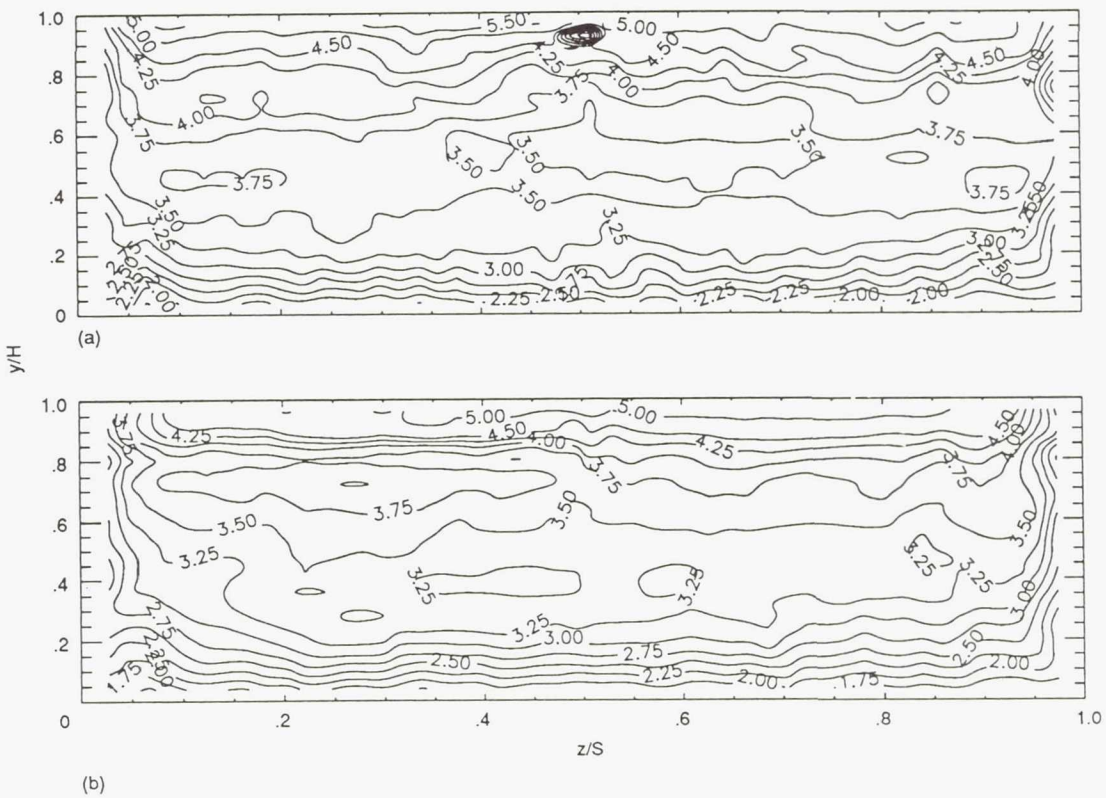

(a) Cowl entrance survey. (b) Cowl exit survey.

Figure 28.—Cross-plane Mach number contours for Lewis/Langley channel flow model at Mach 6.0, $\delta_{h/c}$ = 3.82 cm, and Re = 17.2×10^6/m.

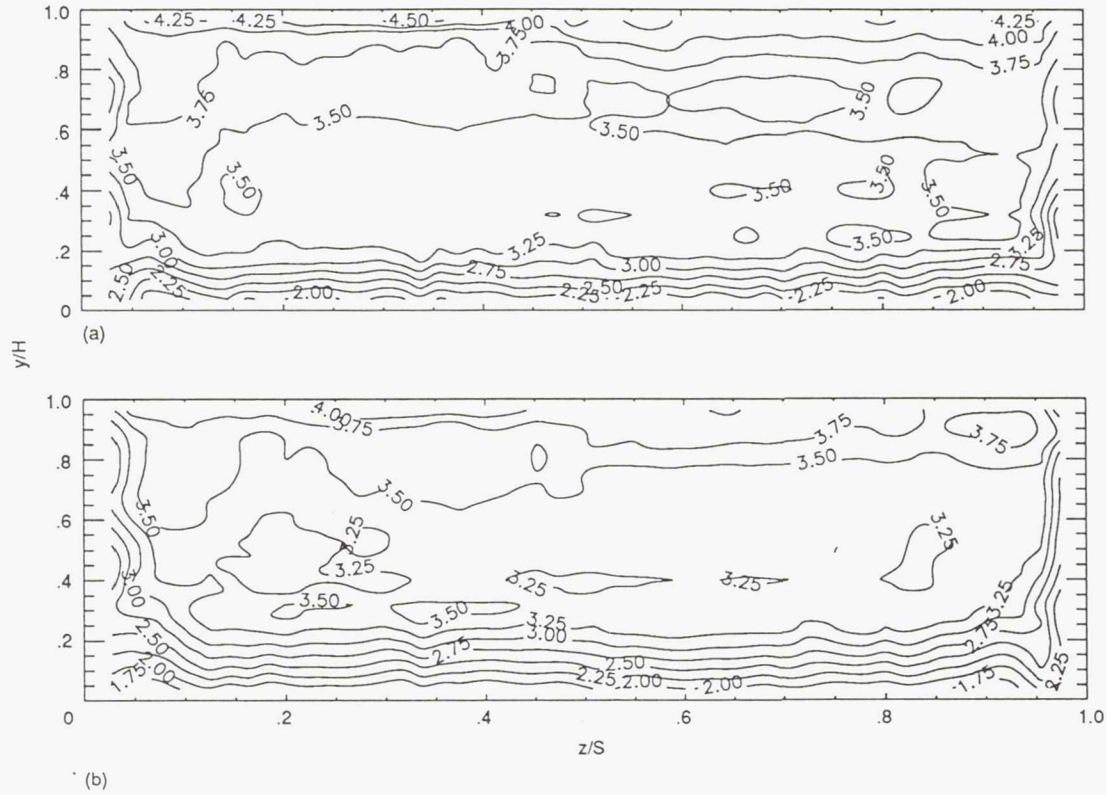

(a) Cowl entrance survey. (b) Cowl exit survey.

Figure 29.—Cross-plane Mach number contours for Lewis/Langley channel flow model at Mach 6.0, $\delta_{h/c}$ = 5.07 cm, and Re = 17.2×10^6/m.

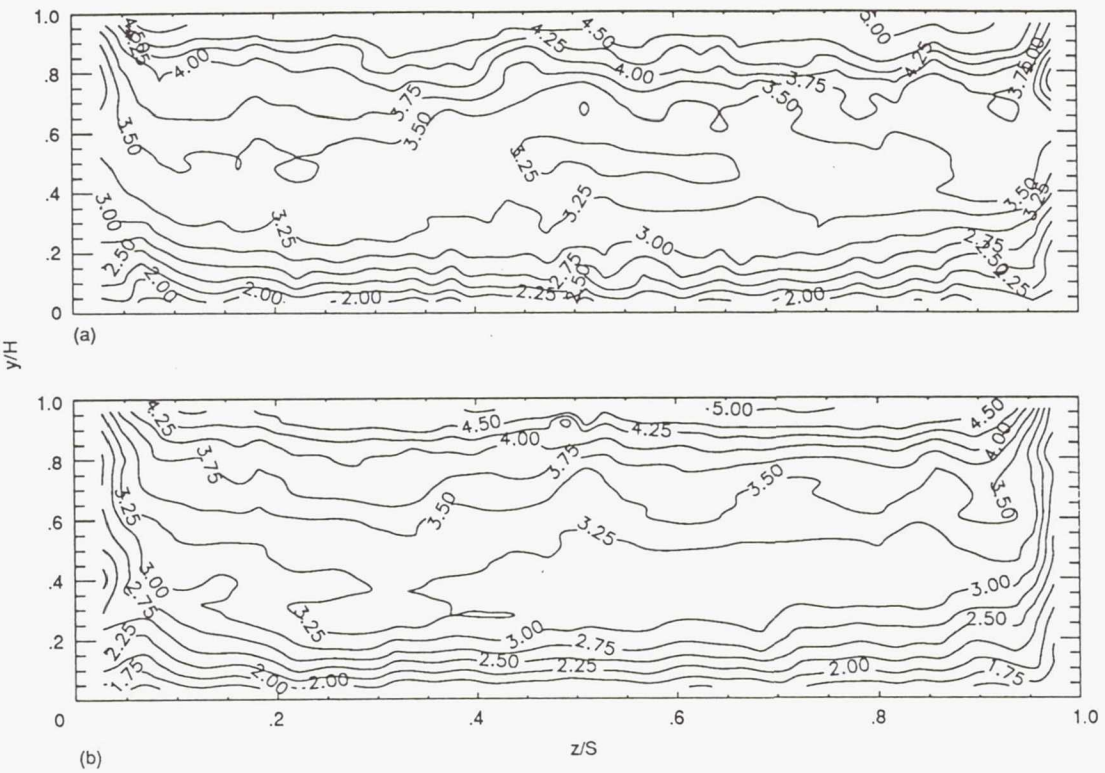

(a) Cowl entrance survey. (b) Cowl exit survey.

Figure 30.—Cross-plane Mach number contours for Lewis/Langley channel flow model at Mach 6.0, $\delta_{h/c}$ = 3.82 cm, and Re = 13.1×10^6/m.

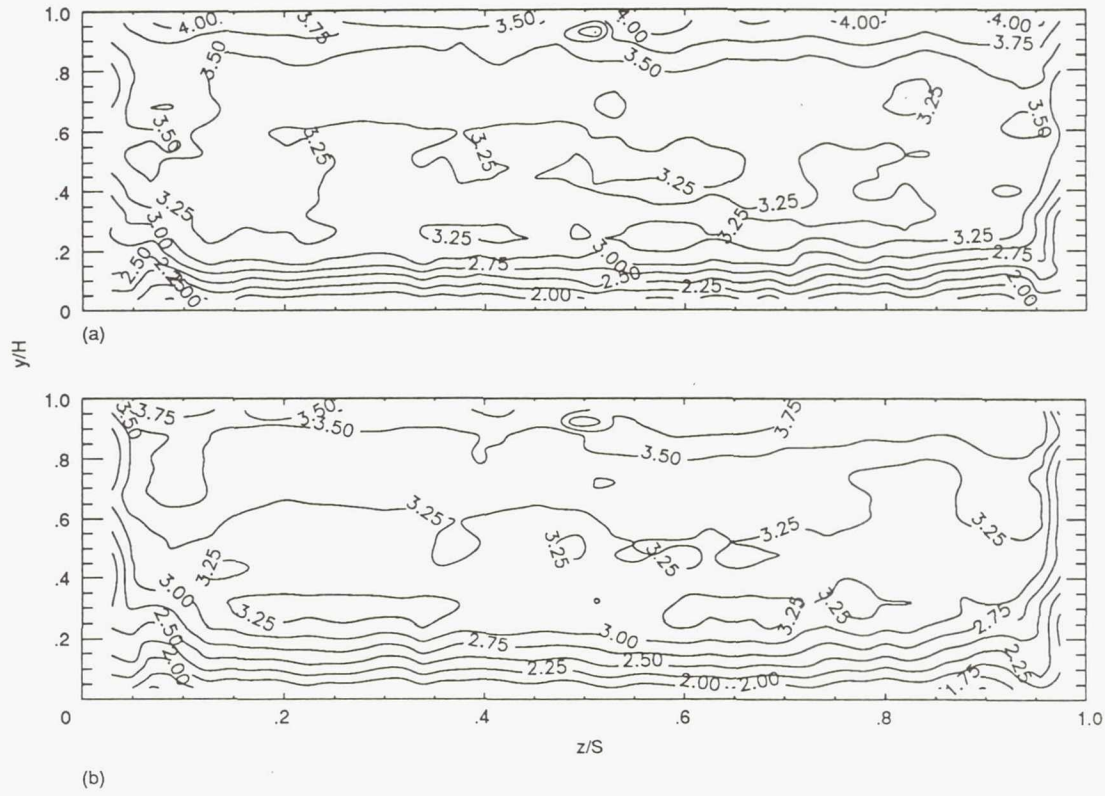

(a) Cowl entrance survey. (b) Cowl exit survey.

Figure 31.—Cross-plane Mach number contours for Lewis/Langley channel flow model at Mach 6.0, $\delta_{h/c}$ = 5.07 cm, and Re = 1.3×10^6/m.

with Reynolds number. Based on the contour results, the generated boundary layer thicknesses are approximately 25 to 30 percent of channel height, and the generated boundary layers do thicken slightly as they develop through the channel.

Concluding Remarks

A program has been established to demonstrate the feasibility of using a contoured honeycomb model to generate an artificially thickened boundary layer in supersonic and hypersonic flows. The use of a contoured honeycomb to selectively remove momentum from the free-stream flow allows one to create a specific boundary layer profile, unlike previous techniques used.

The results of the first configuration, the isolated boundary layer simulator model, indicate that the honeycomb boundary layer simulator can be used to duplicate the momentum distribution of a naturally occurring turbulent boundary layer. However, the boundary layers created by this technique were thinner than expected since they did not span the full boundary layer simulator height. Also, the resulting turbulence levels were much lower than what was seen in a naturally occurring turbulent boundary layer.

The second configuration applied the artificially thickened boundary layer generation process to a channel flow model which was used to simulate an internal flow application. Both pure channel flow and oblique-shock—boundary-layer interactions were investigated. The results indicated similar trends in the channel flow physics for the simulated boundary layer when compared to a naturally occurring, ingested, thick boundary layer. Flow separation due to a strong shock impinging on the thick ingested boundary layer occurred at the same test conditions for both the artificial and natural boundary layer. Also, the losses due to the flow mixing process downstream of the honeycomb boundary layer simulator were quantified. The results indicated that the boundary layer simulation technique was more efficient at lower Mach numbers.

The objectives of the third test phase were to extend the simulated boundary layer channel flow testing to hypersonic conditions and also investigate Reynolds number effects. The larger channel dimensions allowed flow-field surveys farther downstream than in the previous experiments. The results did not indicate a substantial Reynolds number variation in the flow fleld, and the essential trends in the flow physics were retained; that is, the channel floor and sidewall boundary layers had similar shapes and thicknesses. Flow-field surveys made farther downstream than in the previous investigations

indicated that the artificially generated boundary layers become well-behaved, as evidenced by the smoothness of the cross-plane Mach number contours relative to earlier results. The Mach number losses seen at Mach 6.0 due to the boundary layer generation process followed the loss trend of the channel flow data at lower Mach numbers.

The use of the forebody boundary layer simulation technique does produce Mach number losses. Therefore, in a wind tunnel experiment, the tunnel must be run in an overspeed mode in order to get the proper free-stream Mach number and boundary layer profile downstream of the boundary layer simulator. However, a major advantage of this technique is that the compactness of the contoured honeycomb boundary layer simulator allows relatively easy integration into existing wind tunnel model hardware.

Lewis Research Center
National Aeronautics and Space Administration
Cleveland, Ohio, November 30, 1990

References

1. Klebanoff, P.S.; and Diehl, Z.W.: Some Features of Artificially Thickened Fully Developed Turbulent Boundary Layers With Zero Pressure Gradient. NACA Report 1110, 1952.
2. Johnson, D.F.; and Mitchell, G.A.: Experimental Investigation of Two Methods for Generating an Artificially Thickened Boundary Layer. NASA TM X-2238, 1971.
3. Skebe, S.A.: Experimental Investigation of Two-Dimensional Shock Boundary Layer Interactions. Ph.D. Thesis, Case Western Reserve University, Cleveland, OH, 1983.
4. Goldberg, T.J.; and Hefner, J.N.: Starting Phenomena for Hypersonic Inlets With Thick Turbulent Boundary Layers at Mach 6. NASA TN D-6280, 1971.
5. Jurkovich, M.S.; Greber, I.; and Hingst, W.R.: Flow Visualization Studies of a 3-D Shock/Boundary Layer Interaction in the Presence of a Non-Uniform Approach Boundary Layer. AIAA Paper 84-1560, June 1984.
6. Rose, W.C.: The Behavior of a Compressible Turbulent Boundary Layer in a Shock-Wave-Induced Adverse Pressure Gradient. NASA TN D-7092, 1973.
7. Sun, C.C.; and Childs, M.E.: Wall-Wake Velocity Profile for Compressible Nonadiabatic Flows. AIAA J., vol. 14, June 1976, pp. 820-822.
8. Davis, D.O.; and Gessner, F.B.: Further Experiments on Supersonic Turbulent Flow Development in a Square Duct. AIAA J., vol. 27, Aug. 1989, pp. 1023-1030.
9. Johnson, D.A.; and Rose, W.C.: Laser Velocimeter and Hot-Wire Anemometer Comparison in a Supersonic Boundary Layer. AIAA J., vol. 13, Apr. 1975, pp. 512-515.
10. Zoric, D.L.: Approach of Turbulent Boundary Layer to Similarity. Ph.D. Thesis, Colorado State University, Fort Collins, CO, 1968.
11. Ames Research Center Staff: Equations, Tables, and Charts for Compressible Flow. NACA Report 1135, 1953.

NASA
National Aeronautics and Space Administration

Report Documentation Page

1. Report No.	2. Government Accession No.	3. Recipient's Catalog No.
NASA TP-3142		

4. Title and Subtitle

Evaluation of a Technique To Generate Artificially Thickened Boundary Layers in Supersonic and Hypersonic Flows

5. Report Date

August 1991

6. Performing Organization Code

7. Author(s)

A.R. Porro, W.R. Hingst, D.O. Davis, and A.B. Blair, Jr.

8. Performing Organization Report No.

E-5660

10. Work Unit No.

505-80-21

9. Performing Organization Name and Address

National Aeronautics and Space Administration
Lewis Research Center
Cleveland, Ohio 44135-3191

11. Contract or Grant No.

13. Type of Report and Period Covered

Technical Paper

12. Sponsoring Agency Name and Address

National Aeronautics and Space Administration
Washington, D.C. 20546-0001

14. Sponsoring Agency Code

15. Supplementary Notes

A.R. Porro and W.R. Hingst, NASA Lewis Research Center. D.O. Davis, University of Washington, Seattle, Washington 98195 and Summer Student Intern at NASA Lewis Research Center. A.B. Blair, Jr., NASA Langley Research Center, Hampton, Virginia 23665-5225.

16. Abstract

The feasibility of using a contoured honeycomb model to generate a thick boundary layer in high-speed, compressible flow has been investigated. The contour of the honeycomb was tailored to selectively remove momentum in a minimum of streamwise distance to create an artificially thickened turbulent boundary layer. Three wind tunnel experiments were conducted to verify the concept. The first experiment documented the momentum profile and turbulence levels of an artificially thickened boundary layer when tested at nominal Mach numbers of 3.0, 3.5, and 4.0. The second experiment used the concept to generate a thick boundary layer in a channel flow configuration at the same Mach numbers. Oblique-shock—boundary-layer interactions were investigated, along with pure channel flow. Comparisons were made between the simulated boundary layer and a thick, naturally occurring turbulent boundary layer. The third experiment extended the application of the technique to Mach 6. Both schlieren and surface oil flow visualization were used to qualitatively assess the performance of the honeycomb boundary layer simulator. Surface static pressures, together with pitot pressure, static pressure, and hot-wire anemometry flow-field measurements were used to quantify the performance of the boundary layer simulation technique. Results indicate that this technique is a viable concept, especially for high-speed inlet testing applications. In addition, the compactness of the honeycomb boundary layer simulator allows relatively easy integration into existing wind tunnel model hardware. However, Mach number and total pressure losses associated with the boundary layer simulation process must be considered when using the technique.

17. Key Words (Suggested by Author(s))	18. Distribution Statement
Wind tunnels; Boundary layer technology; Fluid flow; Supersonic flow; Hypersonic flow	Unclassified – Unlimited Subject Category 02

19. Security Classif. (of this report)	20. Security Classif. (of this page)	21. No. of pages	22. Price*
Unclassified	Unclassified	32	A03

NASA FORM 1626 OCT 86

*For sale by the National Technical Information Service, Springfield, Virginia 22161

NASA-Langley, 1991